$$\mathcal{S} \rceil \sqsubseteq \rceil \nabla \dashv \updownarrow \quad \mathcal{C} \langle \dashv \wr \sqcup \rangle \rfloor \quad \mathcal{N} \wr \sqcup \rceil \int$$

$\mathcal{S}\rceil\sqsubseteq\rceil\nabla\dashv\updownarrow\,\mathcal{C}\langle\dashv\wr\sqcup\rangle\rfloor\,\mathcal{N}\wr\sqcup\rceil\int$ = `$\cal Several\ Chaotic\ Notes$`

$\mathcal{SEVERAL\ CHAOTIC\ NOTES}$ = `$\cal SEVERAL\ CHAOTIC\ NOTES$`

Ctirad Matyska

Outline:

- Non-linear systems of (ordinary) differential equations and their chaotic behavior in Hamiltonian and dissipative systems (eigenvalues of the Jacobi matrix, Lyapunov exponents)
- Bifurcations and attracting sets: point sets, periodic orbits, tori, strange attractors
- **Parameters in mantle convection models**
- **Bifurcations of stationary solutions, periodic orbits and route to chaos in simple convection systems**
- **Spectra of time series observed in chaotic systems**
- **Fractal dimensions of attractors as a measure of chaoticity**

Geophysical motivation I: Rays as the example of a conservative system

The propagation of rays can be described by means of *the Hamilton canonical equations*

$$\dot{q}_i = \frac{\partial H}{\partial p_i} \,, \quad \dot{p}_i = -\frac{\partial H}{\partial q_i} \tag{1}$$

in six-dimensional phase-space, where the Hamiltonian is equal to half of the eigenvalue of the Christoffel matrix. The phase-space coordinates are formed by generalized coordinates and the slowness vector components.

Local geometrical aspects of ray propagation can be studied by means of *the eigenvalues of the Jacobi matrix* for a fixed propagation time and global geometrical aspects of ray propagation for long times can be studied by means of the analyses of *the propagator matrix*—namely *the Lyapunov exponents*.

Ia. Local exponential behavior of rays

Consider a general Hamiltonian ray tracing system written formally,

$$\frac{dw_i}{dt} = F_i(\mathbf{w}) \ , \quad i = 1, 2, \ldots, N \ , \tag{2}$$

where $N = 6$ ($N = 4$) for 3-D (2-D) problems and w_i are the phase-space coordinates. The ray tracing system (2) is *Hamiltonian* and thus **it preserves phase-space volume** during time evolution (*Liouville's theorem*).

Let $\mathbf{w}(t; \mathbf{w}^0)$ is the ray satisfying (2) and the initial condition $\mathbf{w} = \mathbf{w}^0$ at $t = 0$. We are interested in the behavior of rays in the neighbourhood of a selected ray $\mathbf{w}(t; \mathbf{w}^0)$. In a smooth medium F_i are continuously differentiable; after employing the Taylor expansion and Einstein's summation rule, we may rewrite the system (2) into

$$\frac{d}{dt}(w_i + \delta w_i) \doteq F_i(\mathbf{w}) + \left.\frac{\partial F_i}{\partial w_j}\right|_{\mathbf{w}} \delta w_j \ . \tag{3}$$

Eqn. (2) then immediately yields

$$\frac{d}{dt}\delta w_i \doteq \left.\frac{\partial F_i}{\partial w_j}\right|_{\mathbf{w}} \delta w_j \ . \tag{4}$$

As F_i are smooth, we can write for a selected ray $\mathbf{w}(t;\mathbf{w}^0)$ and a fixed time τ

$$\left.\frac{\partial F_i}{\partial w_j}\right|_{\mathbf{w}(t;\mathbf{w}^0)} = \left.\frac{\partial F_i}{\partial w_j}\right|_{\mathbf{w}(\tau;\mathbf{w}^0)} \quad \text{for} \;\; t \to \tau \;, \tag{5}$$

and the solution of (4) for $t \to \tau$ is

$$\delta\mathbf{w}(t) \doteq \exp[(t-\tau)\boldsymbol{D_F}(\mathbf{w}(\tau;\mathbf{w}^0))] \cdot \delta\mathbf{w}(\tau) \;, \tag{6}$$

where the *Jacobi matrix* $\boldsymbol{D_F}$ and $\exp(\boldsymbol{D_F})$ are

$$(D_F)_{ij}(\mathbf{w}) = \left.\frac{\partial F_i}{\partial w_j}\right|_{\mathbf{w}} \;, \quad \exp(t\boldsymbol{D_F}) = \sum_{n=0}^{\infty} \frac{1}{n!}(t\boldsymbol{D_F})^n \;. \tag{7}$$

To construct N independent solutions of the studied linearized system we determine eigenvalues λ and eigenvectors $\mathbf{e}$ of the matrix $\boldsymbol{D_F}$. Eigenvalues and eigenvectors are introduced by the relation

$$(\boldsymbol{D_F} - \lambda\boldsymbol{I})\mathbf{e} = \mathbf{0} \;, \tag{8}$$

where $\boldsymbol{I}$ is the identity matrix. In general, the Jacobi matrix is not symmetric and thus both eigenvalues and eigenvectors can be complex.

If $\boldsymbol{D_F}$ has N linearly independent eigenvectors $\mathbf{e}_j$, $j = 1, 2, \ldots, N$, then the independent solutions of (4) are simply $\exp(\alpha_j t)\mathbf{e}_j$, where α_j is an eigenvalue corresponding to $\mathbf{e}_j$. If we have a pair of complex conjugate eigenvalues α_j, α_{j+1} with the corresponding complex eigenvectors, a pair $\exp(\Re\alpha_j t)[\cos(\Im\alpha_j t)\Re\mathbf{e}_j - \sin(\Im\alpha_j t)\Im\mathbf{e}_j]$, $\exp(\Re\alpha_j t)[\sin(\Im\alpha_j t)\Re\mathbf{e}_j + \cos(\Im\alpha_j t)\Im\mathbf{e}_j]$ represents linearly independent real solutions. Here $\Re$ denotes real and $\Im$ imaginary part of the complex numbers.

First summary:

The time dependence of rays in the neighbourhood of a selected ray at a particular time $t = \tau$ can thus be exponential. This local behavior is controlled by the real parts of **the eigenvalues of the Jacobi matrix**. If there are no multiple eigenvalues, the phase-space E_N is divided into the three linearly independent subspaces, E^s, E^u and E^c, where the *stable subspace* E^s is spanned by the eigenvectors whose eigenvalues have negative real parts, the *unstable subspace* E^u is spanned by the eigenvectors whose eigenvalues have positive real parts and the *center subspace* E^c is spanned by the eigenvectors whose eigenvalues have zero real parts. Each of the subspaces is invariant under the time evolution of the linearized system (4), (5), i.e., the solutions lying in E^s are characterized by exponential decay, those lying in E^u by exponential growth, and those lying in E^c by neither of these cases (see also Guckenheimer and Holmes, 1983). *This analysis is, however, valid only for a short-time evolution of rays near a selected phase-space point.*

Ib. Global chaotic behavior of rays

The real parts of eigenvalues $\Re\alpha_j$ are given by the inverse of a time unit, which means that they do not depend on a spatial unit chosen to describe a studied ray tracing model. Since the ray tracing system preserves phase-space volume during time evolution either $E^c = E_N$ or both E^s and E^u have positive dimensions. Let us number the eigenvalues α_j so that α_N is the eigenvalue with the largest real part. Then $(\Re\alpha_N)^{-1}$ represents the *local characteristic time of predictability* of ray behavior.

The exponential amplification of small perturbations δw_i can result in a *sensitive dependence on initial conditions* for long times. However, the Jacobi matrix $\boldsymbol{D_F}$ can change along rays, i.e., $\boldsymbol{D_F}$ is a function of time for a selected ray $\mathbf{w}(t;\mathbf{w}^0)$ and thus such a global instability need not occur under the presence of local instabilities.

Suppose now that we deal with a model with both geometrically smooth interfaces and smooth material properties outside the interfaces so that $\mathbf{w}(t;\mathbf{w}^0)$ smoothly depends on $\mathbf{w}^0$. Employing again the Taylor expansion and Einstein's summation rule, we may write

$$w_i(t;\mathbf{w}^0+\delta\mathbf{w}^0) \doteq w_i(t;\mathbf{w}^0) + \frac{\partial w_i}{\partial w_j^0}(t;\mathbf{w}^0)\delta {w^0}_j \ , \tag{9}$$

where

$$\Pi_{ij}(t;\mathbf{w}^0) \equiv \frac{\partial w_i}{\partial w_j^0}(t;\mathbf{w}^0) \tag{10}$$

is the *propagator matrix* of a selected ray. The expansion (9) can be rewritten into the form

$$\delta\mathbf{w}(t;\mathbf{w}^0;\delta\mathbf{w}^0) \doteq \mathbf{\Pi}(t;\mathbf{w}^0)\cdot\delta\mathbf{w}^0 \ . \tag{11}$$

The propagator matrix can thus be used to analyze the chaoticity of rays due to both a spatial-dependence of material properties outside the interfaces and undulations of the interfaces. Both these effects can lead to an exponential divergences of rays in the phase-space, which can be globally described by means of the exponents formally corresponding to the eigenvalues of the Jacobi matrix $\boldsymbol{D_F}$ in the cases with constant $\boldsymbol{D_F}$ along a ray.

Definition (see also Lanford, 1981): The point $\mathbf{w}^0$ has **the Lyapunov** (or *characteristic*) **exponents** $\lambda_1 < \lambda_2 < \ldots < \lambda_N$ if there exist subspaces $E_1 \subset E_2 \subset \ldots \subset E_N$, with each E_k of dimension k, such that

$$E_k = \left\{ \mathbf{u} \in E_N; \limsup_{t\to\infty} \frac{1}{t} \ln ||\mathbf{\Pi}(t;\mathbf{w}^0)\,\mathbf{u}|| \le \lambda_k \right\} \tag{12}$$

and

$$\limsup_{t\to\infty} \frac{1}{t} \ln ||\mathbf{\Pi}(t;\mathbf{w}^0)\,\mathbf{u}|| = \lambda_k \quad \text{if } \mathbf{u} \in E_k \text{ but } \mathbf{u} \notin E_{k-1} \ . \tag{13}$$

Numerical evaluation of Lyapunov exponents

There is a problem in numerical computations that the components of the phase-space represent different physical quantities (generalized coordinates and generalized slowness vector components). Although the above definition of the Lyapunov exponents does not depend on the scaling of w_i, we are not able to operate with infinitely long time-series. Finite-time guesses of the Lyapunov exponents are then dependent on a choice of the scalar product generating the employed norm.

The largest Lyapunov exponent can be numerically computed by a random choice of $\mathbf{u}$ in the expression $t^{-1} \ln ||\mathbf{\Pi}(t; \mathbf{w}^0)\, \mathbf{u}||$ (see Keers et al., 1997). Since the subspace (12) corresponding to λ_N is the basic space E_N, there is zero probability that randomly chosen $\mathbf{u}$ is from the $(N-1)$-dimensional space E_{N-1}. Hence, (13) is satisfied for $k = N$. However, in practical applications we can only estimate λ_N on a finite-time interval. It is, therefore, useful to estimate $t^{-1} \ln ||\mathbf{\Pi}(t; \mathbf{w}^0)\, \mathbf{u}||$ for several randomly chosen $\mathbf{u}$ with unit modulus under the selected norm.

Remark

We may also try to find the Lyapunov exponents λ_k as the limits

$$\lambda_k = \limsup_{t \to \infty} \frac{1}{t} \ln |\sigma_k(t)| \ , \tag{14}$$

where $\sigma_k(t)$ are the eigenvalues of the propagator matrix, or even in a simplified version of (14), where $\limsup_{t\to\infty}$ is replaced by only $\lim_{t\to\infty}$. However, in dynamic ray tracing models $(1/t)\ln|\sigma_k(t)|$ can be a function oscillating over a finite interval (Klimeš, personal communication). Hence we deal with the limiting behavior of an upper envelope of $(1/t)\ln|\sigma_k(t)|$.

Correlations

Definition: Correlation matrix of phase-space velocities $\boldsymbol{C}(\tau;\mathbf{w}^0)$ has the elements

$$C_{ij}(\tau;\mathbf{w}^0)=\lim_{T\to\infty}\frac{1}{T}\left[\int_0^T F_i(\mathbf{w}(t;\mathbf{w}^0))F_j(\mathbf{w}(t+\tau;\mathbf{w}^0))\,dt\right.$$
$$\left.-\frac{1}{T}\int_0^T F_i(\mathbf{w}(t;\mathbf{w}^0))\,dt\int_0^T F_j(\mathbf{w}(t+\tau;\mathbf{w}^0))\,dt\ .\right] \tag{15}$$

In many chaotic systems $|C_{ij}|$ decay exponentially with the time-shift τ. The decay coefficient can be then viewed similarly as the Lyapunov exponent—its inverse is the characteristic time of predictability of the orbit behavior near the selected orbit $\mathbf{w}(t;\mathbf{w}^0)$.

Second summary:

The Lyapunov exponents represent the rate of exponential growth or damping of infinitesimal displacements for $t \to \infty$, i.e., the inverse of the largest positive Lyapunov exponent gives the *global characteristic time of predictability* of ray behavior near a selected ray, i.e., the Lyapunov exponents are the quantities associated with a particular ray $\mathbf{w} = \mathbf{w}^0$ at $t = t^0$. This is the reason why a simple quantification of a whole model by, e.g., the largest Lyapunov exponent found, may result in a deep misunderstanding of the basic physics of the model because we thus obtain the characteristic time of predictability of ray propagation near only the ray corresponding to this exponent.

The Poincaré sections

The Poincaré sections represent a tool enabling to transfer original dynamic system to iterative maps. Let S be an $(N-1)$-dimensional surface "transverse" to the trajectories of a dynamical system. Let x_0 be a point on S at time t_0; for any point x_0, where the trajectory starting at x_0 returns to S after certain time intervals, we obtain a mapping

$$\mathbf{w}^1 = P(\mathbf{w}^0)\,, \quad \mathbf{w}^2 = P(\mathbf{w}^1)\,, \quad \ldots \quad \mathbf{w}^n = P(\mathbf{w}^{n-1}) \quad \ldots\,. \tag{16}$$

The mapping P is called *the return map* or *the Poincaré map* of the dynamical system and the chaotic properties of the original system can be studied by means of such a map.

"Interface" iterative maps and rays

In ray propagation, an additional effect to that caused by smoothly heterogeneous media is the effect of undulating interfaces. In such a case it is possible to restrict the attention to the values of phase-space coordinates of a selected ray at instants of its incidence on chosen interfaces. In other words, these incidences define again a discrete map

$$\mathbf{w}^{(i+1)} = \mathbf{G}(\mathbf{w}^{(i)}) \ . \tag{17}$$

Let us confine our considerations only to the special problems when we study the repeated incidence of a ray on the same interface. Then we can redefine the phase-space coordinates since the location of the selected interface in the real space can be parameterized by means of some parameters s_j, $j = 1, ..., N/2 - 1$ and the incidence of a ray by the angles s_j, $j = N/2, ..., N - 2$ and

$$\mathbf{w}^{(i)} = \mathbf{w}^{(i)}(\mathbf{s}). \tag{18}$$

This relation describes a parametrization of a cross-section in the original phase-space. On this section we have a map

$$s_j^{(i+1)} = G_j(s_1^{(i)}, \ldots, s_{N-2}^{(i)}) \, . \tag{19}$$

A sequence of points $\{\mathbf{s}^{(i)}\}_{i=-\infty}^{\infty}$ in E_{N-2} is then called an *orbit*. Each interface with infinitely repeated incidences of the ray represents the special case of *Poincaré sections*. *Chaotic behavior of rays can be visualized* by drawing orbits in such a cross-section of the original phase-space.

F1 - vlnovod a biliár

The *Lyapunov exponents* associated with a selected orbit can be defined by only a slight change of the previous definition for continuous time: the time t is replaced by the number of iteration i and the propagator matrix $\mathbf{\Pi}(t; \mathbf{w}^0)$ is replaced by the Jacobi matrix $\boldsymbol{D}_{\boldsymbol{G}}^{\boldsymbol{i}}(\mathbf{s}^{(0)})$ of the i-th iteration of the procedure starting at $\mathbf{s} = \mathbf{s}^{(0)}$. It is clear that $\boldsymbol{D}_{\boldsymbol{G}}^{\boldsymbol{i}}(\mathbf{s}^{(0)}) = \boldsymbol{D}_{\boldsymbol{G}}(\mathbf{s}^{(i-1)})\boldsymbol{D}_{\boldsymbol{G}}(\mathbf{s}^{(i-2)})\ldots\boldsymbol{D}_{\boldsymbol{G}}(\mathbf{s}^{(0)})$, where $\boldsymbol{D}_{\boldsymbol{G}}(\mathbf{s}^j)_{kl} = \partial G_k(\mathbf{s}^j)/\partial s_l$.

Visualization of orbits on such a Poincaré section can sometimes distinctly separate regions with chaotic and regular behavior without any quantification.

Geophysical motivation II: Thermal convection as the example of a dissipative chaotic system

Consider a system written formally in the same way,

$$\frac{dw_i}{dt} = F_i(\mathbf{w}) \ , \quad i = 1, 2, \ldots, N \ . \tag{20}$$

However, $N \to \infty$ now because (20) arises from discretization of a problem of continuum (thermo)mechanics.

Denote again $\mathbf{w}(t, \mathbf{w}^0)$ the solution (*orbit*) of (20) satisfying $\mathbf{w} = \mathbf{w}^0$ at $t = 0$. The description of dynamical system by means of orbits can be viewed as an analog of Lagrangian description of particle motions in continuum mechanics and $d\mathbf{w}/dt$ is thus an analog of a velocity field (for $N \gg 1$ instead of $N = 2$ or $N = 3$). Choose a phase-space volume $V(t)$ in any time t, then

$$\frac{dV}{dt} = \int_{V(t)} \nabla \cdot \frac{d\mathbf{w}}{dt} \, dV \ . \tag{21}$$

In dissipative systems $\nabla \cdot \mathbf{w} \ll 0$ and the space-phase volume is shrinking in (almost) all directions during evolution; nevertheless, there may exist positive Lyapunov exponents and thus close orbits may exponentially diverge in several directions.

Attracting sets and attractors

The set $\mathcal{A}$ is called *an attracting set with fundamental neighbourhood* $\mathcal{U}$, if:

- for every open set $\mathcal{V} : \mathcal{A} \subset \mathcal{V}$ there exists time t_0 such that orbits $\mathbf{w}(t > t_0, \mathbf{w}^0) \in \mathcal{V} \ \ \forall\ \mathbf{w}^0 \in \mathcal{U}$ (*attractivity*)
- $\mathbf{w}(t, \mathbf{w}^0) \in \mathcal{A} \ \ \forall\ \mathbf{w}^0 \in \mathcal{A}$ (*invariance*)

Usually some kind of *irreducibility* is required so that $\mathcal{A}$ may be called *an attractor*.
Note: two orbits lying in $\mathcal{A}$ may (locally) exponentially diverge. F2 - atrahujici mnozina

Examples of attractors (and saddles and repellors)

Stationary points $\mathbf{w}_s$ are solutions of the equation $\mathbf{F}(\mathbf{w}_s) = 0$.
Periodic solutions $\mathbf{w}_p(t)$ satisfy the relation $\mathbf{w}_p(t) = \mathbf{w}_p(t + T)$ for some period T.
Torus is created if there are at least two periods T_1 and T_2 such that T_2/T_1 is an irrational number.
Strange attractors have non-integer (fractal) dimension which is usually low for real physical systems (only several degrees of freedom!).

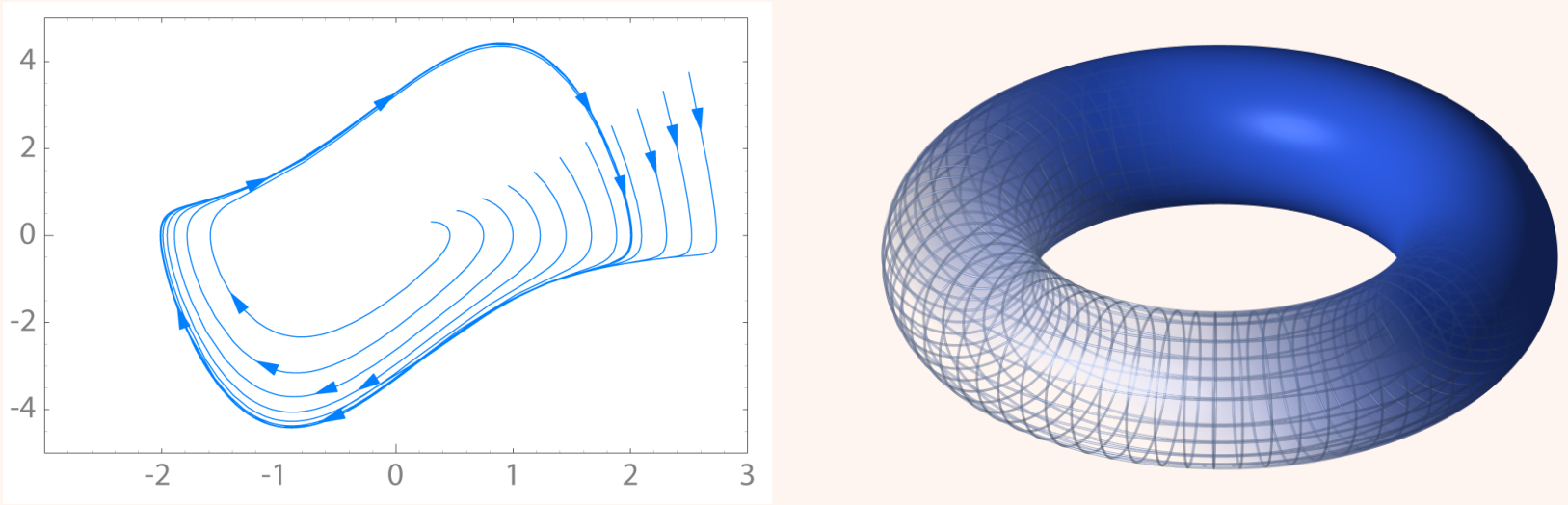

Figure 1: Stable periodic attractor (van der Pol equation: $y'' - \mu(1 - y^2)y' + y = 0$) and torus.

Local stability analysis
of an orbit can be again performed employing the (huge!) *Jacobi matrix*:

Stationary points:
Eqns. (3) and (4) attain the simpler form

$$\frac{d}{dt}(\mathbf{w}_s + \delta\mathbf{w}) \doteq \nabla \boldsymbol{F}\big|_{\mathbf{w}_s} \cdot \delta\mathbf{w}, \tag{22}$$

$$\frac{d}{dt}\delta\mathbf{w} \doteq \nabla \boldsymbol{F}\big|_{\mathbf{w}_s} \cdot \delta\mathbf{w} \tag{23}$$

The Jacobi matrix is now evaluated in the fixed point $\mathbf{w}_s$:
If all its eigenvalues have negative real parts, $E^s = E_N$ and $\mathbf{w}_s$ is a point attractor.
If all its eigenvalues have positive real parts, $E^u = E_N$ and $\mathbf{w}_s$ is a point repellor (not a typical case).
If $\dim E^s > 0$ and $\dim E^u > 0$, and $\dim E^c = 0$, $\mathbf{w}_s$ is a saddle (typical unstable stationary solution).
If $\dim E^c > 0$ the situation is more complicated, in the systems with controlling parameters a bifurcation occurs.

Periodic orbits and tori:
The Jacobi matrix is now time-dependent similarly as for the rays.

Figures from:

M. Marek and I. Schreiber: *Chaotic Behaviour of Deterministic Dissipative Systems*, Academia and Cambridge Univ. Press, Praha 1991.

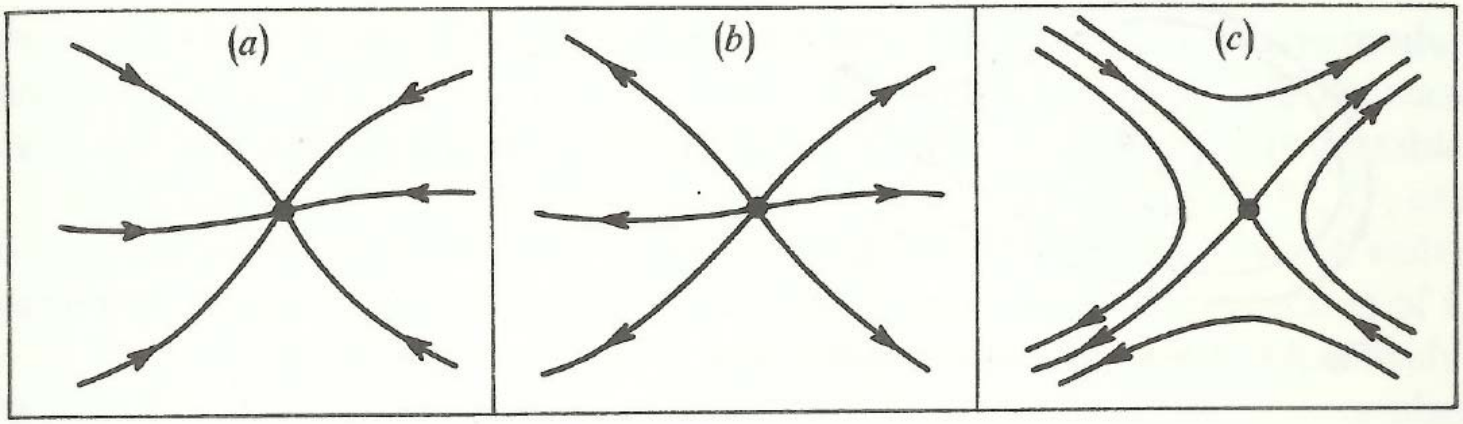

Fig. 2.3. Hyperbolic stationary points: (*a*) attractor; (*b*) repellor; (*c*) saddle.

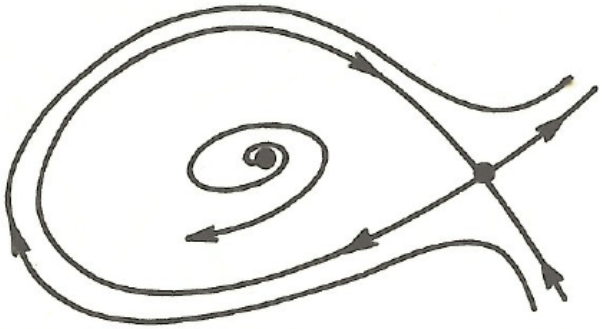

Fig. 2.4. A homoclinic orbit or saddle loop.

Bifurcations

It is common that the studied systems are dependent on some real parameters $\alpha_1, \alpha_2, \ldots, \alpha_M$, i.e., formally

$$\frac{d\mathbf{w}}{dt} = \mathbf{F}(\mathbf{w}, \boldsymbol{\alpha}) \ , \quad \mathbf{w} \in E_N \ , \quad \boldsymbol{\alpha} \in E_M \ . \tag{24}$$

Structure of orbits depends on $\boldsymbol{\alpha}$. *Bifurcation* occurs when orbit structure changes qualitatively with a variation of $\boldsymbol{\alpha}$ at a *critical* (bifurcation) *value* $\boldsymbol{\alpha} = \boldsymbol{\alpha}_c$.

Bifurcations of stationary points:
$(M = 1) \Longrightarrow$ isolated $\boldsymbol{\alpha}_c$ exist when either a unique zero real eigenvalue or a pair of purely imaginary eigenvalues of $\boldsymbol{D_F} \equiv \nabla \mathbf{F}|_{\mathbf{w}_s}$ appear.
$(M = 2) \Longrightarrow$ bifurcation curves are studied, where most of the points correspond to single degenerate $\boldsymbol{D_F} \equiv \nabla \mathbf{F}|_{\mathbf{w}_s}$ but there may be also points with double degenerate Jacobi matrix.
$(M > 2) \Longrightarrow$ more and more complicated situations may be present.
Examples: *saddle node, symmetry breaking, transcritical and Hopf bifurcations.*

Bifurcations of periodic orbits:
Examples: *period-doubling, periodic orbit* $\longrightarrow$ *torus*

Figures from:

M. Marek and I. Schreiber: *Chaotic Behaviour of Deterministic Dissipative Systems*, Academia and Cambridge Univ. Press, Praha 1991.

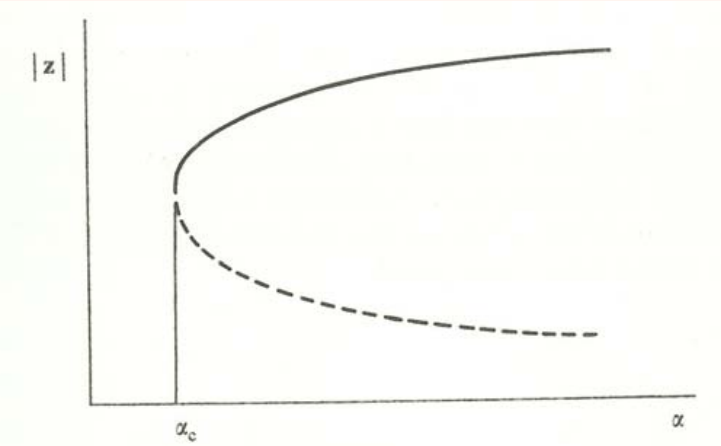

Fig. 3.3. Saddle-node bifurcation.

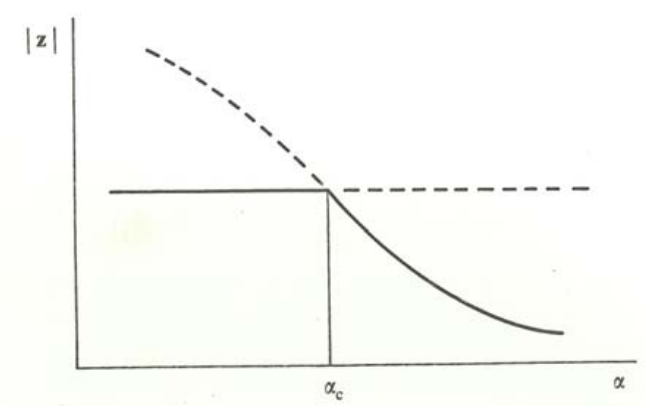

Fig. 3.5. Transcritical bifurcation.

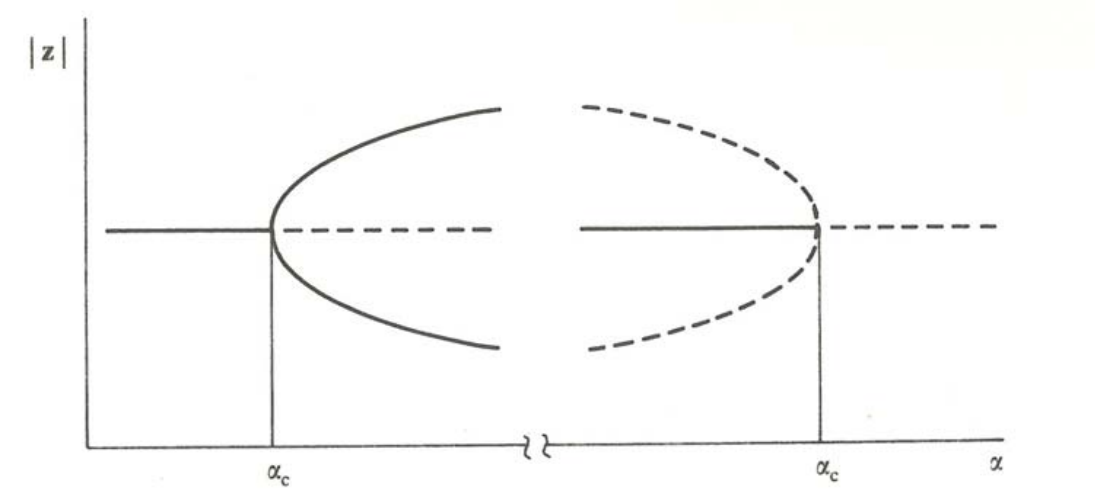

Fig. 3.4. Symmetry breaking bifurcation; supercritical (left) and subcritical (right) cases are shown.

Figures from:

M. Marek and I. Schreiber: *Chaotic Behaviour of Deterministic Dissipative Systems*, Academia and Cambridge Univ. Press, Praha 1991.

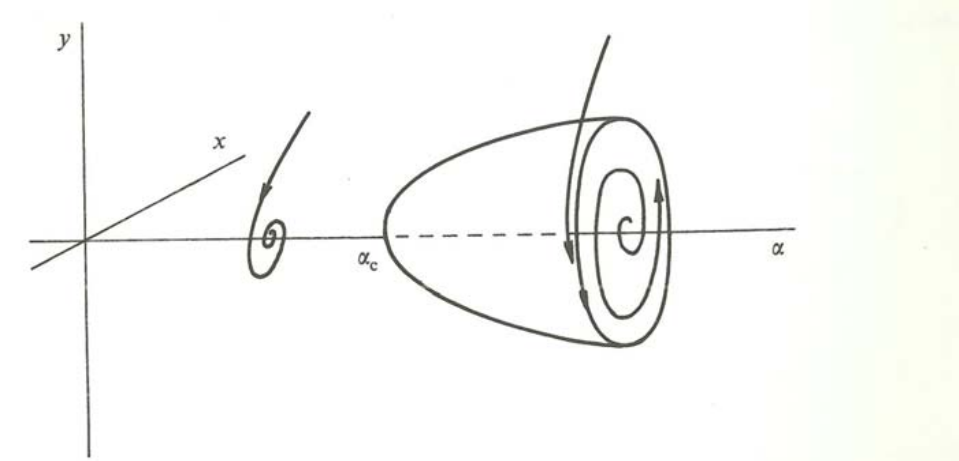

Fig. 3.7. Hopf bifurcation in the product space $R^2 \times R$. The one-parameter family of periodic orbits lies on a paboloid.

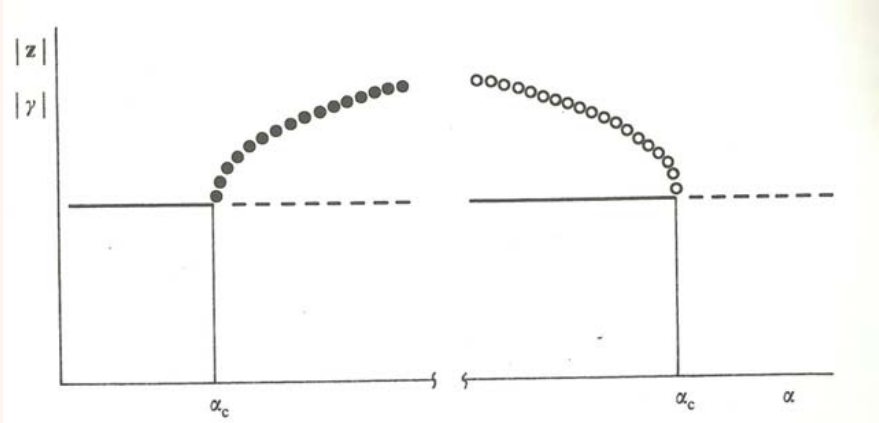

Fig. 3.6. Hopf bifurcation; supercritical (left) and subcritical (right) cases are shown.

Figures from:

M. Marek and I. Schreiber: *Chaotic Behaviour of Deterministic Dissipative Systems*, Academia and Cambridge Univ. Press, Praha 1991.

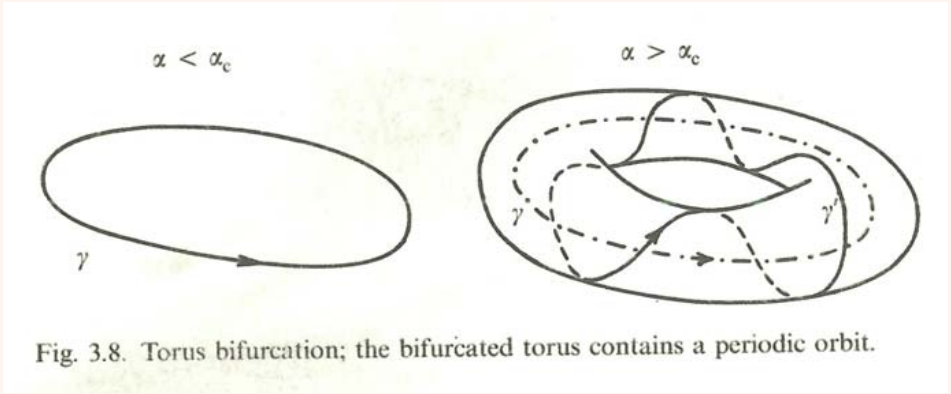

Fig. 3.8. Torus bifurcation; the bifurcated torus contains a periodic orbit.

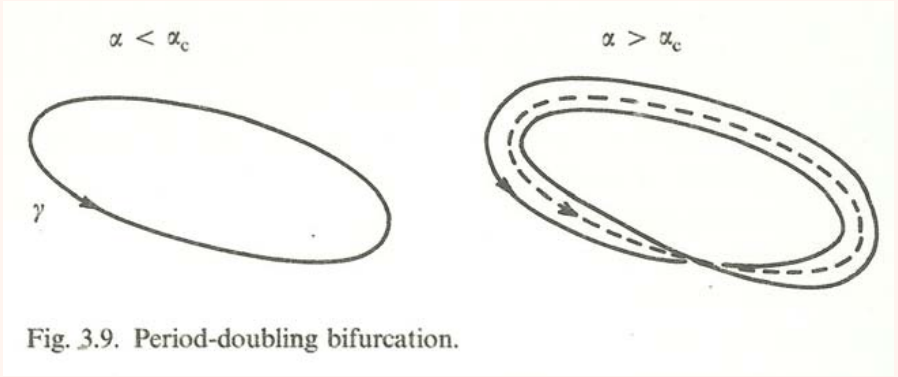

Fig. 3.9. Period-doubling bifurcation.

Figures from:

M. Marek and I. Schreiber: *Chaotic Behaviour of Deterministic Dissipative Systems*, Academia and Cambridge Univ. Press, Praha 1991.

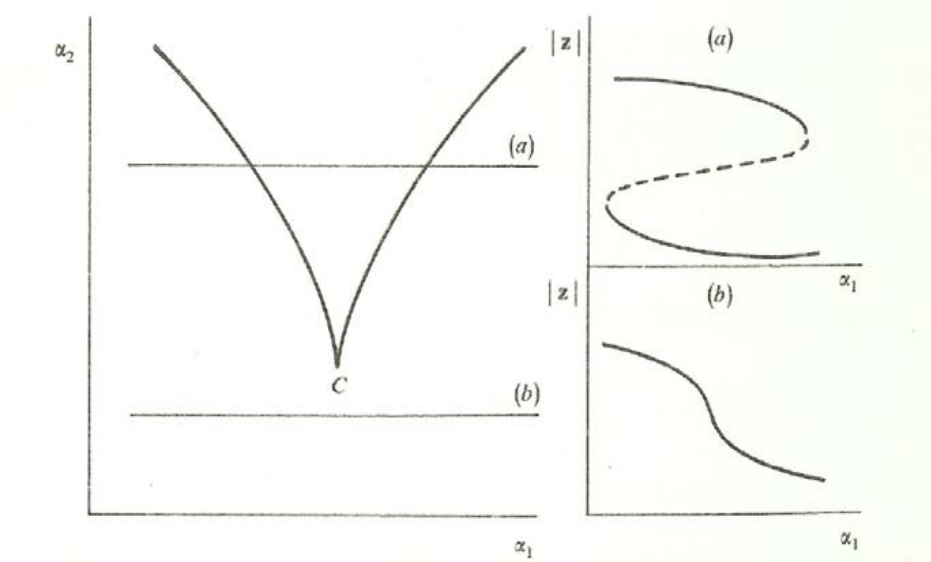

Fig. 3.10. Cusp bifurcation; corresponding solution diagrams along the straight lines (*a*) and (*b*) are shown in the right part of the figure; full lines represent stable stationary points and dashed lines unstable ones.

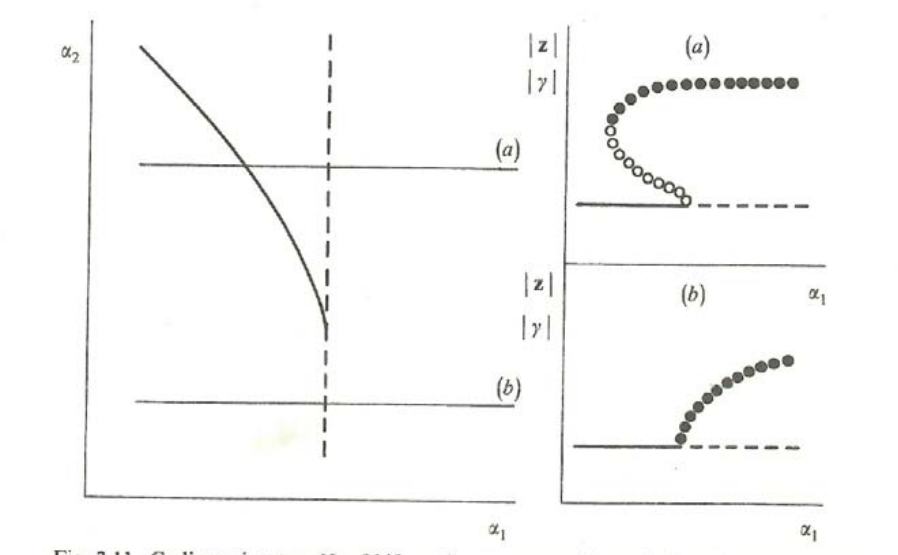

Fig. 3.11. Codimension two Hopf bifurcation; corresponding solution diagrams contain both stationary points (lines) and periodic orbits (circles: solid circles – stable periodic orbits; open circles – unstable periodic orbits).

Parameterization of (mantle) convection models

The laws of conservation written by means of the *dimensionless numbers* are

$$\nabla \cdot \boldsymbol{v} = 0\,, \tag{25}$$

$$-\nabla\Pi + \nabla\cdot\left(\frac{\eta}{\eta_s}(\nabla\boldsymbol{v} + (\nabla\boldsymbol{v})^T)\right) + Ra_s\frac{\alpha}{\alpha_s}(T-T_0)\boldsymbol{e}_r = {Pr_s}^{-1}\left(\frac{\partial\boldsymbol{v}}{\partial t} + \boldsymbol{v}\cdot\nabla\boldsymbol{v}\right)\,, \tag{26}$$

$$\frac{\partial T}{\partial t} = \nabla\cdot\left(\frac{\kappa}{\kappa_s}\nabla T\right) - \boldsymbol{v}\cdot\nabla T + \frac{Raq_s}{Ra_s} - D_s\frac{\alpha}{\alpha_s}\left(T + \frac{T_s}{T_b - T_s}\right)v_r + \frac{D_s}{Ra_s}\frac{\eta}{\eta_s}(\nabla\boldsymbol{v} + (\nabla\boldsymbol{v})^T) : \nabla\boldsymbol{v}, \tag{27}$$

where

the (surface) Prandtl number	$Pr_s = \frac{\nu_s}{\kappa} \quad (Pr \to \infty)$
the (surface) Rayleigh number	$Ra_s = \frac{\alpha_s(T_b - T_s)g_0 d^3}{\nu_s \kappa}$
the (surface) Rayleigh number for heat sources	$Raq_s = \frac{\alpha_s g_0 Q d^5}{\nu_s \kappa k}$
the (surface) dissipation number	$D_s = \frac{\alpha_s g_0 d}{c_p}$

.

Is such a system deterministic in 3-D?

However, not only these four numbers are controlling parameters but also dimensionless functions $\eta/\eta_s,\ \alpha/\alpha_s,\ \kappa/\kappa_s$ (+ phase transitions + iron spin transitions + ...). Is there an infinite number of parameters?

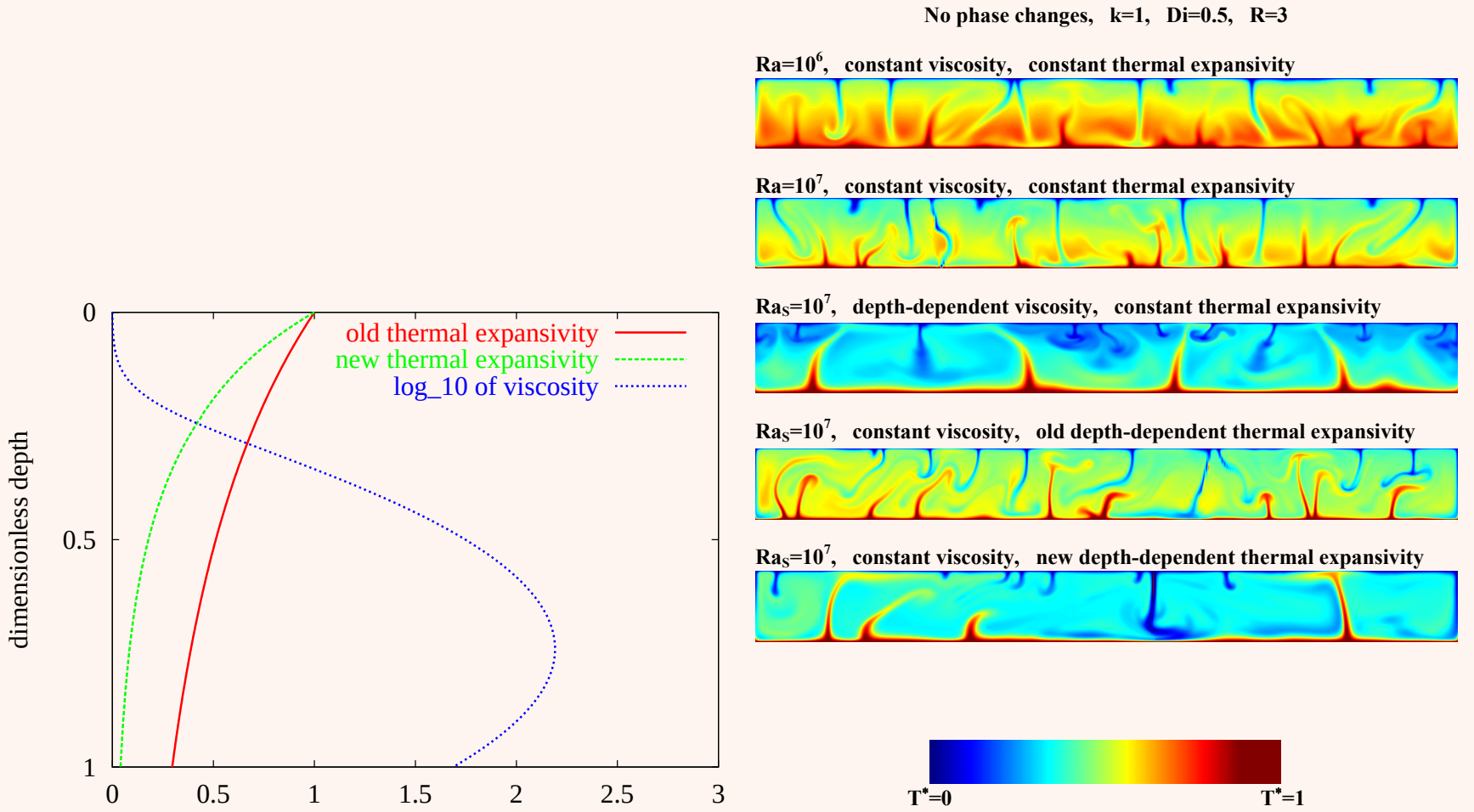

Figure 2: From *Matyska and Yuen, Lower-mantle material properties and convection models of multiscale plumes, The Geological Society of America, Special Paper 430, 2007.*

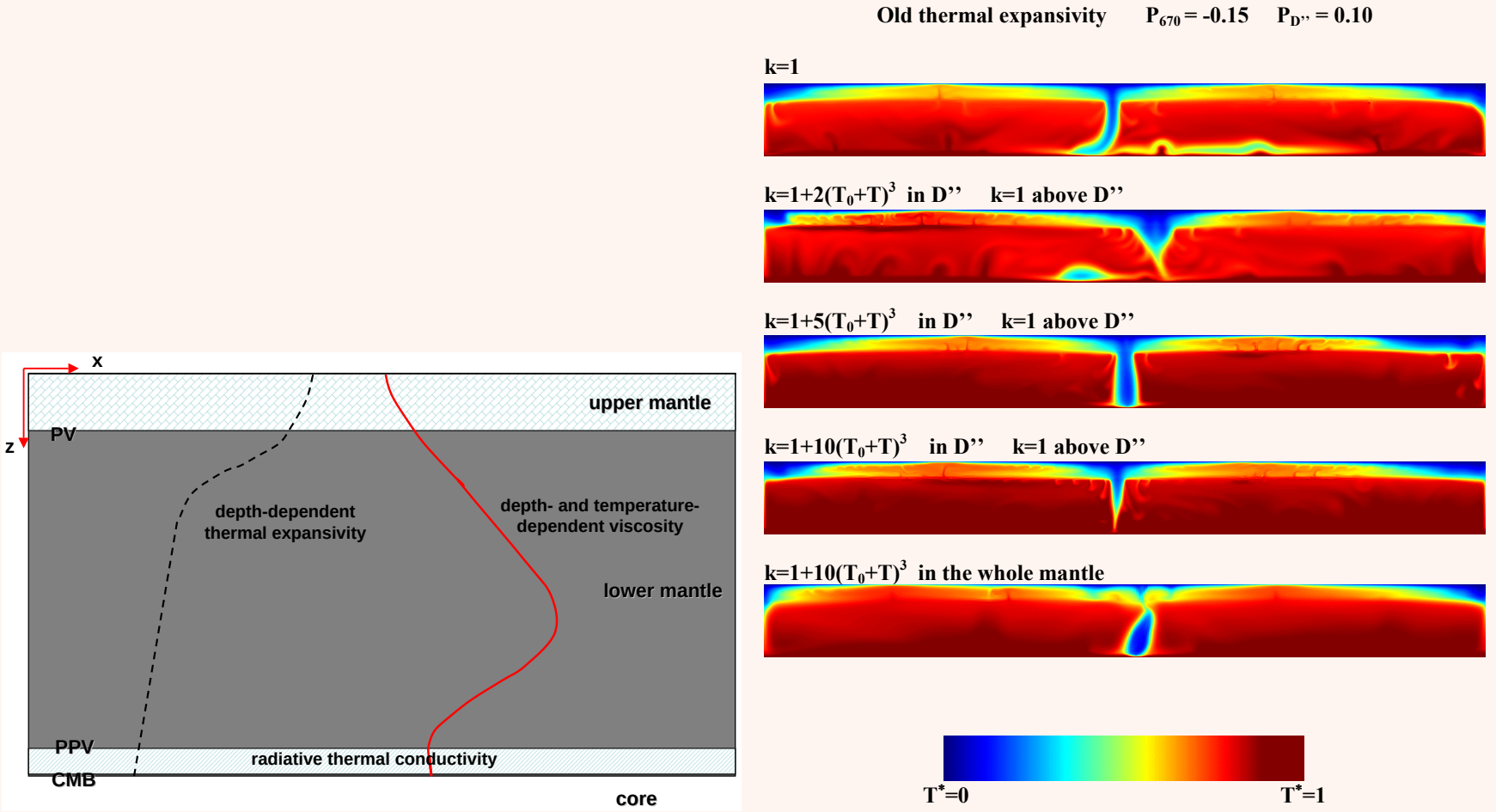

Figure 3: From *Matyska and Yuen, Lower-mantle material properties and convection models of multiscale plumes, The Geological Society of America, Special Paper 430, 2007.*

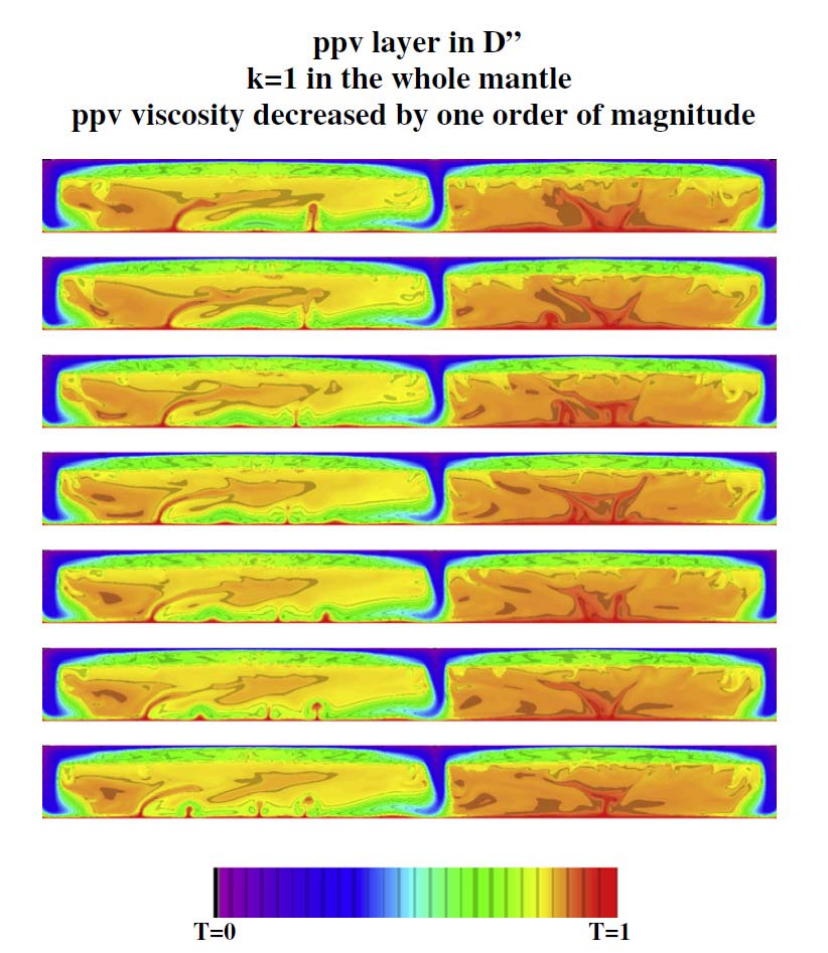

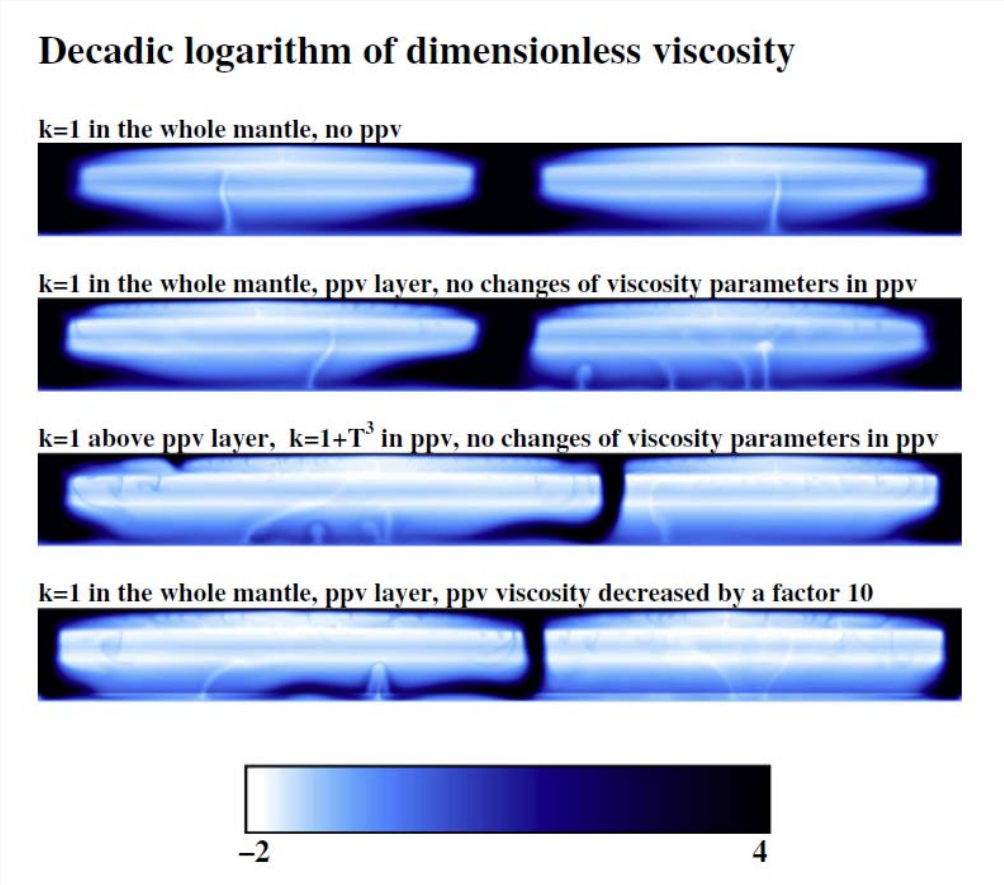

Figure 4: From *Matyska et al., The impact of variability in the rheological activation parameters on lower-mantle viscosity stratification and its dynamics, Phys. Earth Planet. Int., 2011, 188, 1–8.*

The simplest convection system and route to chaos

$$\nabla \cdot \boldsymbol{v} = 0\,, \tag{28}$$

$$-\nabla \Pi + \nabla^2 \boldsymbol{v} + Ra(T - T_0)\boldsymbol{e}_r = Pr^{-1}\left(\frac{\partial \boldsymbol{v}}{\partial t} + \boldsymbol{v}\cdot\nabla\boldsymbol{v}\right)\,, \tag{29}$$

$$\frac{\partial T}{\partial t} = \nabla^2 T - \boldsymbol{v}\cdot\nabla T\,. \tag{30}$$

conductive solution $\longrightarrow$ stable stationary solution $\longrightarrow$ periodic orbit $\longrightarrow$ torus $\longrightarrow$ (Ruelle-Takens-Newhouse, intermittency, period-doubling) $\longrightarrow$

chaos

"Suppose that for there is an attracting fixed point for ($Ra < Ra_1$) that loses its stability in a Hopf bifurcation at $Ra = Ra_1$ (i.e., the fixed point is replaced by an attracting periodic orbit). In addition, suppose that at $Ra = Ra_2 > Ra_1$ there is another Hopf bifurcation to a quasi-periodic orbit (i.e., the attractor is now a torus T^2). A subsequent Hopf bifurcation at $Ra = Ra_3 > Ra_3$ creates a quasi-periodic 3-torus. However, S.E. Newhouse, D. Ruelle and F. Takens showed that for $n \geq 3$ every constant vector field on the torus T^n can be perturbed by an arbitrarily small amount to a new vector field with a chaotic attractor. Thus, in an experiment, one may see a bifurcation from a 2-frequency quasi-periodic flow to a chaotic attractor. This route to turbulence is in contrast to the classical theory of L. Landau and E. Lifshitz, which says that turbulence arises from the successive addition of incommensurate frequences as a parameter is increased." (http://www.encyclopediaofmath.org/index.php/Routes_to_chaos)

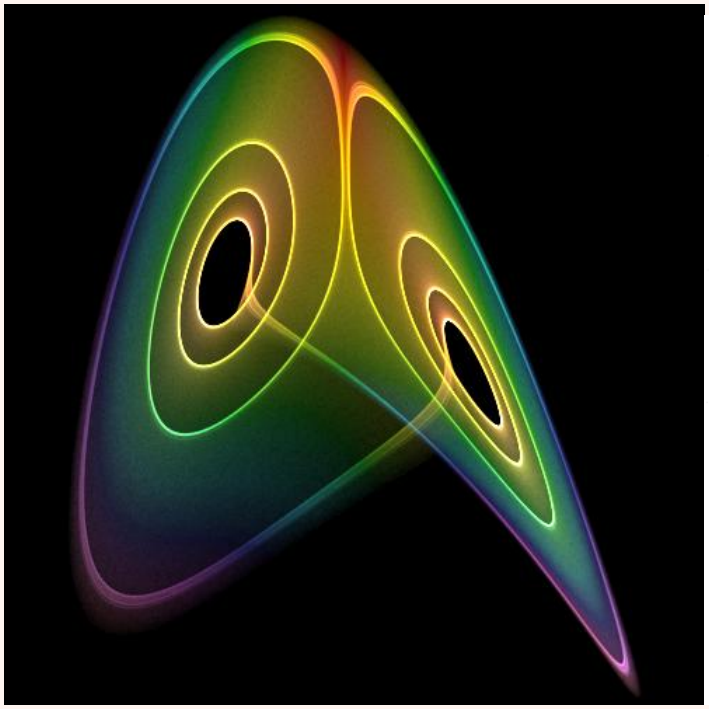

Onset of Chaos in the Rayleigh-Benard Convection

Hideo YAHATA

Department of Materials Science, Hiroshima University, Hiroshima 730

(Received October 1, 1984)

Time evolution of the Rayleigh-Benard convection near the transition to chaos is investigated using Galyorkin systems of ordinary differential equations containing several dozen variables. The small aspect-ratio systems that are confined in a rectangular box or a cylindrical cell are considered. Computations were performed with gradual increase of the Rayleigh number under several chosen values of the Prandtl number, the aspect ratio, the non-Boussinesq parameters and the Taylor number. Depending on the values of these external parameters, the routes to chaos exhibited by the present dynamical systems are as follows: (a) period-doubling cascade; (b) destruction of the two-torus with or without an intervenient phase-locked state; (c) excitation of intermittent bursts. The computational results are compared with those by experimental observations and those for low-dimensional dynamical systems.

Figure 5: Other routes to chaos: intermittency and period-doubling. Left: the Lorenz attractor ($\mathrm{d}A/\mathrm{d}t = Pr(B-A)$, $\mathrm{d}B/\mathrm{d}t = rA - B - A$, $\mathrm{d}C/\mathrm{d}t = -bC + AB$) near an intermittent cycle: much of the time the trajectory is close to a nearly periodic orbit, but diverges and returns. http://commons.wikimedia.org/wiki/Category:Chaoscope

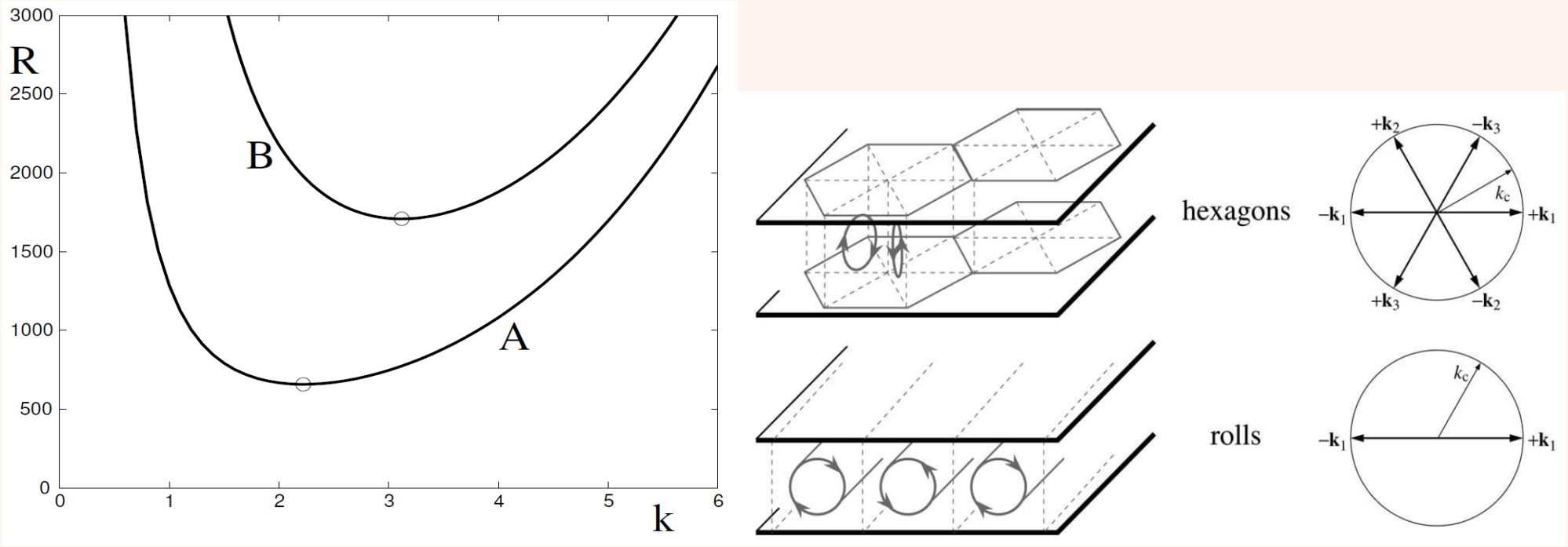

Figure 6: Marginal stability curves for stress-free (A) and no-slip (B) velocity boundary conditions and isothermal plates; hexagons vs. rolls. From *Manneville, Rayleigh-Bénard convection, thirty years of experimental, theoretical, and modeling work, Springer, 2006.*

Let us suppose that velocity does not depend on the y-coordinate and that $v_y = 0$. In this case, we can obtain the solenoidal field satisfying the equation of continuity ($\nabla \cdot \boldsymbol{v} = 0$) by expressing velocity in the form

$$\boldsymbol{v} \equiv (v_x, v_z) = \left(\frac{\partial \psi}{\partial z}, -\frac{\partial \psi}{\partial x} \right) , \tag{31}$$

where $\psi = \psi(x, z)$ is the *stream function*. As

$$\boldsymbol{v} \cdot \nabla \psi = 0 \, , \tag{32}$$

it is clear that the isolines of ψ are the streamlines of velocity.

For the classical Boussinesq approximation without internal heating and with infinite Prandtl number the momentum and heat equations are

$$\nabla^4 \psi = Ra \frac{\partial \Theta}{\partial x} \, , \tag{33}$$

$$\frac{\partial \Theta}{\partial t} = \nabla^2 \Theta - \frac{\partial \psi}{\partial z} \frac{\partial \Theta}{\partial x} + \frac{\partial \psi}{\partial x} \frac{\partial \Theta}{\partial z} - \frac{\partial \psi}{\partial x} \, . \tag{34}$$

If we consider impermeable, free-slip boundary conditions for $z = 0$ and $z = 1$, we obtain the boundary conditions in the form:

$$\Theta = \psi = \frac{\partial^2 \psi}{\partial z^2} = 0 \quad \text{for} \quad z = 0, 1 \, . \tag{35}$$

We can convert the problem into the spectral domain by applying the Fourier transform and sine decomposition as follows,

$$\hat{\psi}(k;z,t) = \frac{1}{\sqrt{2\pi}} \int_{-\infty}^{\infty} \psi(x;z,t) e^{-ikx}\, dx\,, \tag{36}$$

$$\hat{\psi}(k;z,t) = \sum_{n=-\infty}^{\infty} \hat{\psi}_n(k;t) e^{in\pi z}\,, \quad \hat{\psi}_n = -\hat{\psi}_{-n}\,, \tag{37}$$

$$\hat{\Theta}(k;z,t) = \sum_{n=-\infty}^{\infty} i\hat{\Theta}_n(k;t) e^{in\pi z}\,, \quad \hat{\Theta}_n = -\hat{\Theta}_{-n}\,. \tag{38}$$

The solution of the biharmonic equation (33) in the spectral domain is

$$\hat{\psi}_n = \frac{-k\, Ra}{(k^2+n^2\pi^2)^2}\, \hat{\Theta}_n\,. \tag{39}$$

The heat equation (34) attains the form

$$\begin{aligned} \frac{\partial \hat{\Theta}_n}{\partial t} &= \left[-(k^2+n^2\pi^2) + \frac{k^2\, Ra}{(k^2+n^2\pi^2)^2} \right] \hat{\Theta}_n \\ &+ \sum_j \pi\, Ra \left(\frac{-jk\hat{\Theta}_j}{(k^2+j^2\pi^2)^2} * (k\hat{\Theta}_{n-j}) + \frac{(n-j)k^2\hat{\Theta}_j}{(k^2+j^2\pi^2)^2} * \hat{\Theta}_{n-j} \right)\,. \end{aligned} \tag{40}$$

Solution of linear part of eqn. (40) thus depends on the sign of

$$\beta_n(k) = -(k^2 + n^2\pi^2) + \frac{k^2\, Ra}{(k^2 + n^2\pi^2)^2}\ ; \tag{41}$$

clearly $\beta_1 > \beta_2 > \beta_3 \ldots$. Therefore, in this stability analysis it is sufficient to deal with β_1 only. It is clear that $\beta_1 < 0\ \forall k \Leftrightarrow Ra < (k^2 + \pi^2)^3/k^2\ \forall k$. Let us find the minimum of the function $f(k) = (k^2 + \pi^2)^3/k^2$. As $\partial f/\partial k = k^{-4}(6k^3(k^2 + \pi^2)^2 - 2k(k^2 + \pi^2)^3)$, f attains its minimum in $k_m = \pi/\sqrt{2}$; $f(k_m) = \frac{27}{4}\pi^4$.

To conclude: if

$$Ra < Ra_c = \frac{27}{4}\pi^4\,, \tag{42}$$

the transfer of heat due to conduction represents the stable state and no convection arises. However, if the Rayleigh number is greater than the *critical Rayleigh number* Ra_c, convection is generated by fluctuations in the system.

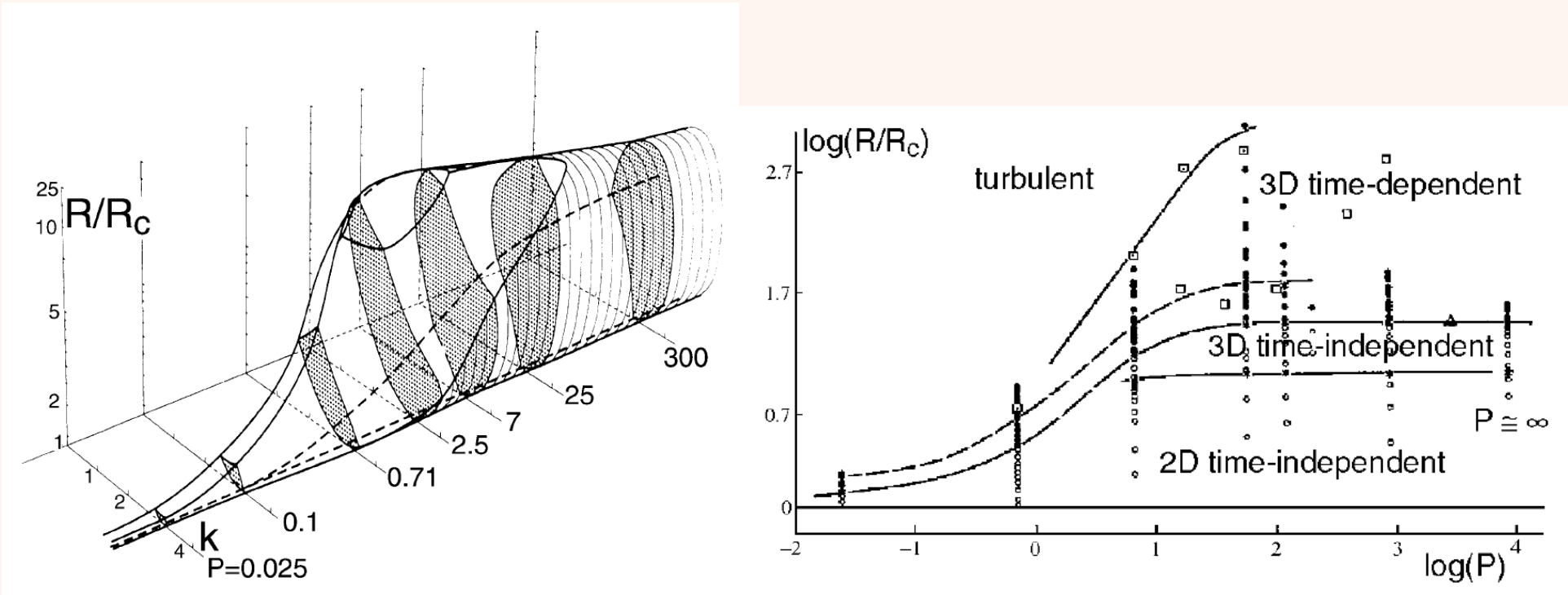

Figure 7: Busse balloon showing stability of rolls (there may exist also non-roll stable solutions) in perspective in the (k; P;R)-space, after Busse (1978); transition to turbulence in RB convection: experimental results collected before 1973 by Krishnamurti (1973). From *Manneville, Rayleigh-Bénard convection, thirty years of experimental, theoretical, and modeling work, Springer, 2006.*

Onset of the Thermal Convection in a Finite Two-Dimensional Box

Jiro MIZUSHIMA

Journal of the Physical Society of Japan
Vol. 64, No. 7, July, 1995, pp. 2420–2432

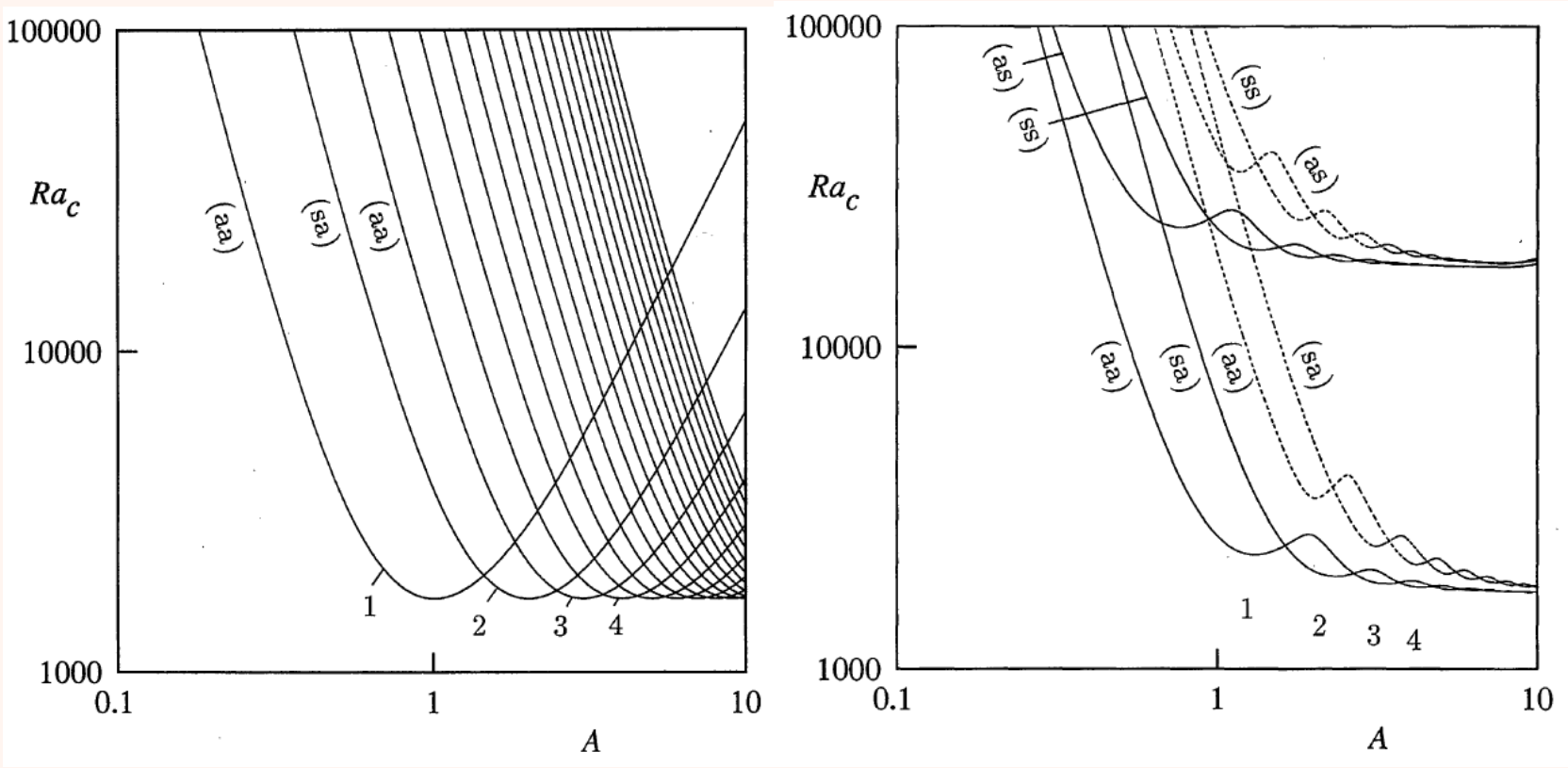

Figure 8: Effect of wavenumbers discretization (A is the aspect ratio of the box). Lower and upper boundaries are rigid and perfectly conducting (isothermal); side walls are perfectly insulating and stress-free (left) or rigid (right).

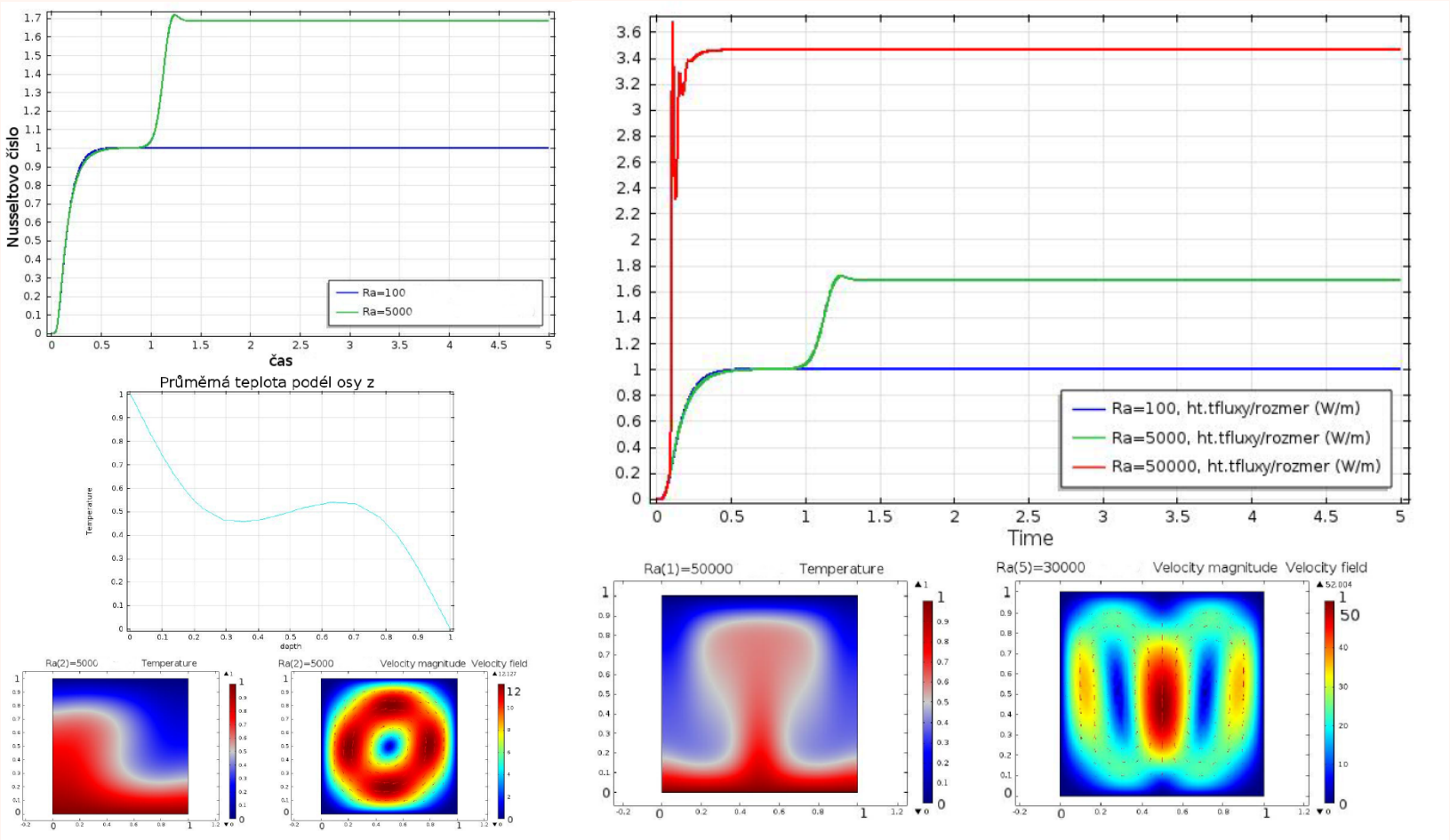

Figure 9: **Stationary solutions:** If the convecting system is bounded by vertical walls, the wavenumbers k become discrete $\Longrightarrow$ additional bifurcations can appear and/or the solutions can attract only locally. Transition from one to two convection rolls is shown here. From *Šustková, Master Thesis, Fac. Math. and Phys., Charles Univ., 2014.*

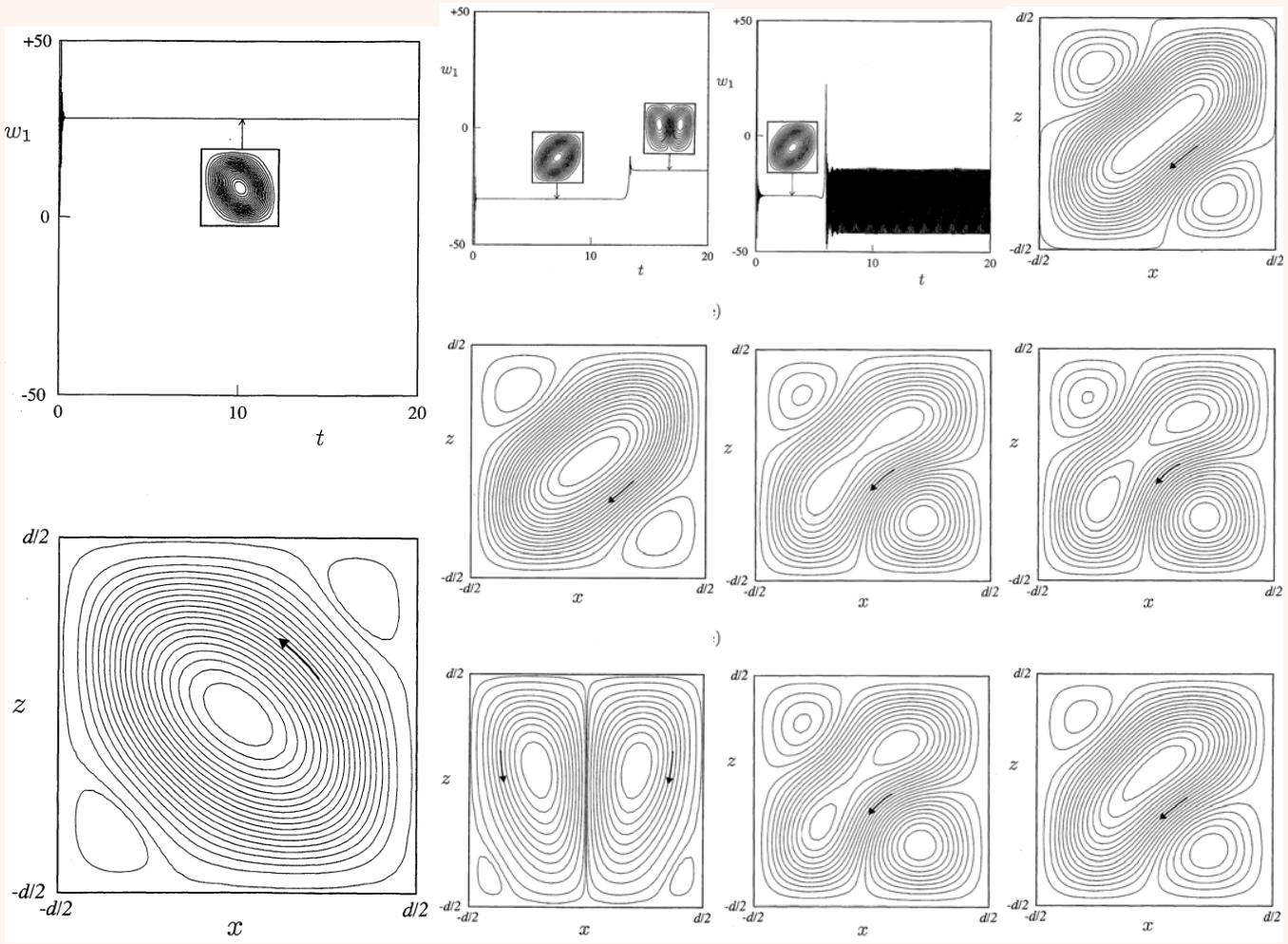

Figure 10: Convection in a square rigid box with perfectly conducting boundaries for Ra = 25000, 40000 and 48000.

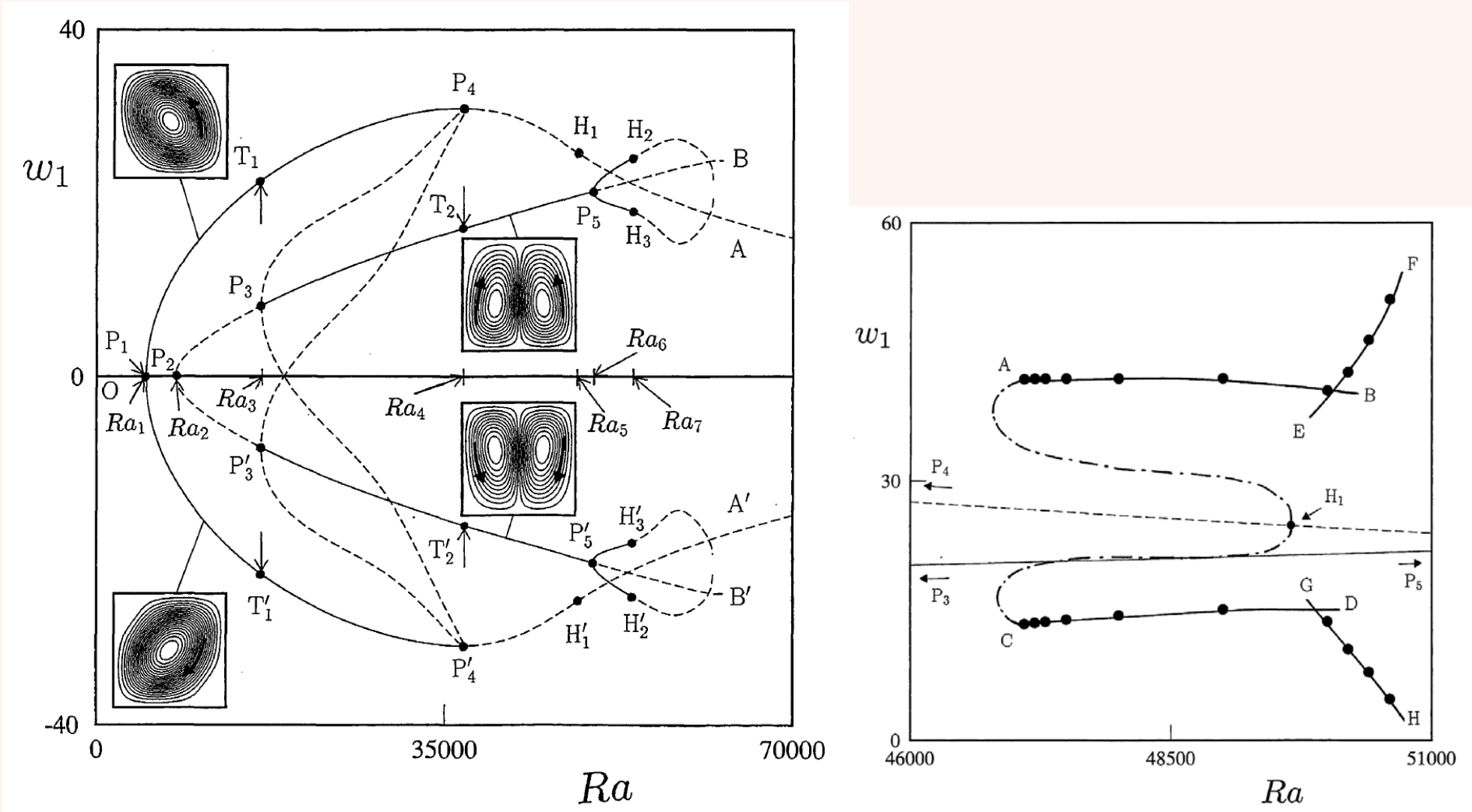

Figure 11: Bifurcation diagram of convection in a square rigid box with perfectly conducting boundaries.

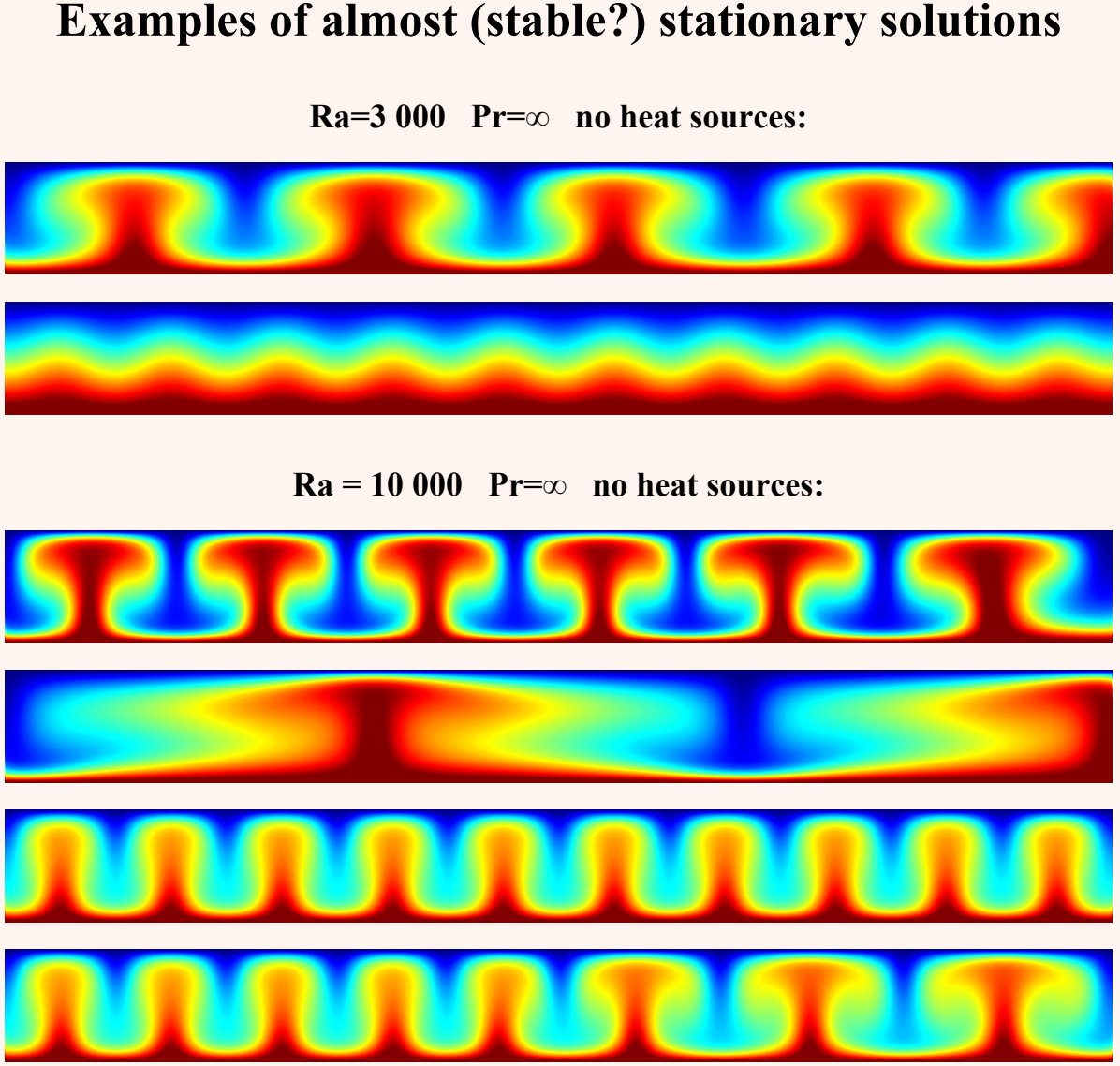

Figure 12: Temperature distribution of convection in classical Boussinesq approximation. All boundaries are impermeable with free slip; top and bottom boundaries are perfectly conducting, side walls are prefectly insulating.

Examples of higher Ra solutions

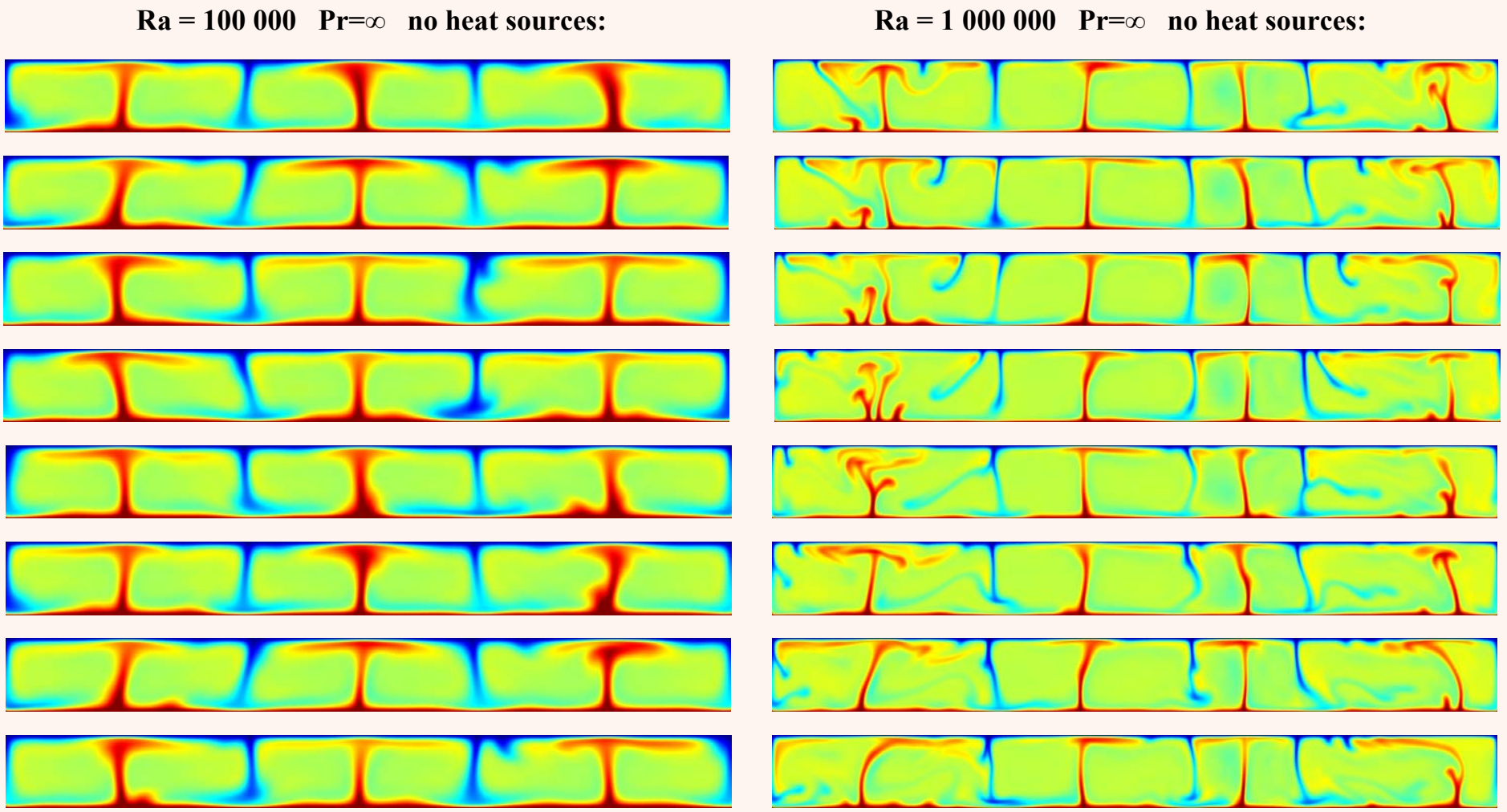

Figure 13: Time sequences of convection temperature distribution in classical Boussinesq approximation. All boundaries are impermeable with free slip; top and bottom boundaries are perfectly conducting, side walls are prefectly insulating.

Examples of high Ra solutions

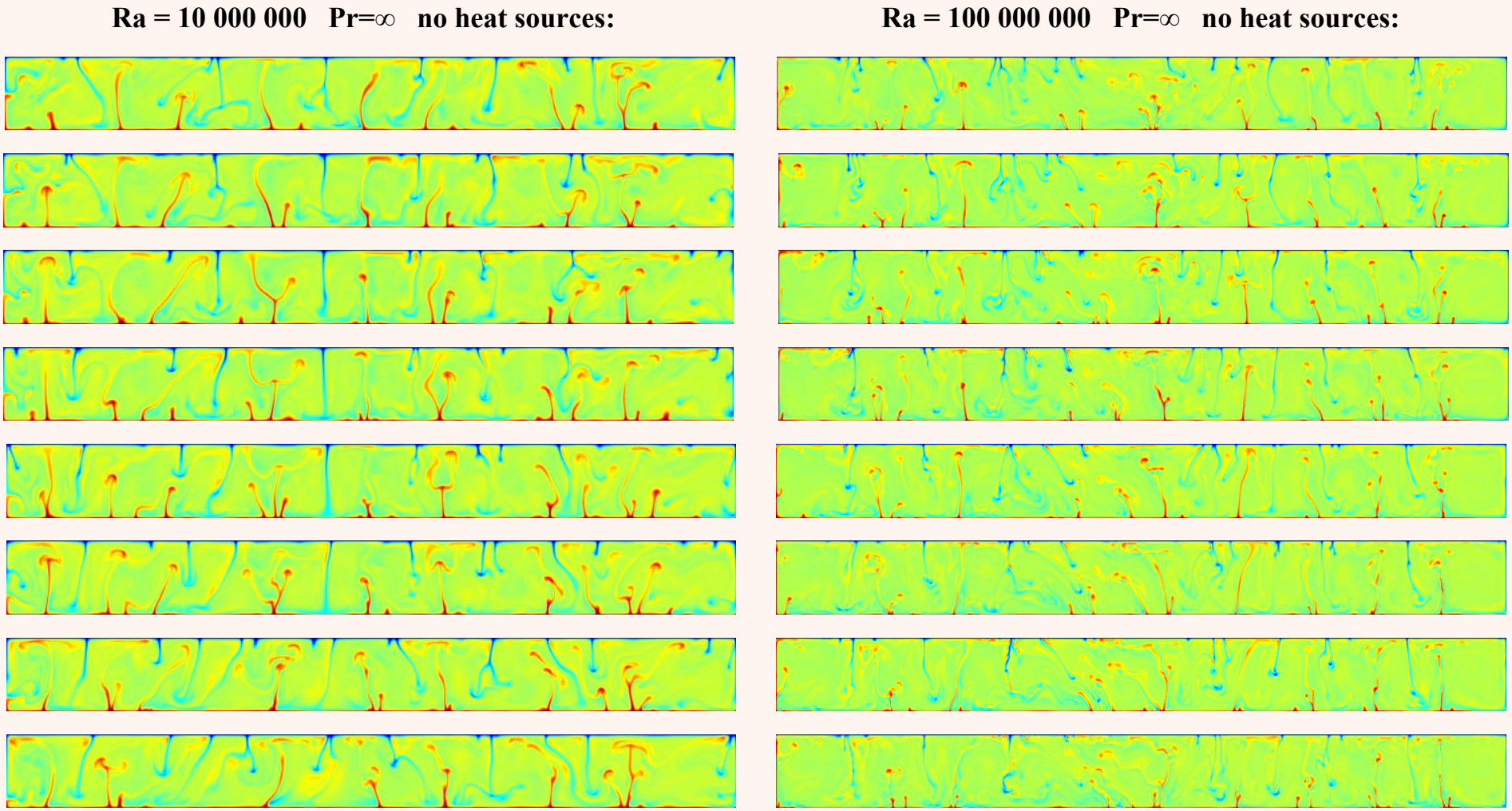

Figure 14: Time sequences of convection temperature distribution in classical Boussinesq approximation. All boundaries are impermeable with free slip; top and bottom boundaries are perfectly conducting, side walls are prefectly insulating.

III. Several questions for those studying Earth-similar complex systems

The Earth is only weakly chaotic (on geological time-scale) $\Longrightarrow$ material properties stabilize the mantle convection; an analysis (i.e. finding critical values of parameters) for complex systems can be performed (only) numerically:

- **How to deal with zoology of (stable) stationary solutions?**
- **How to perform transition from periodic to chaotic solutions for continuos changes of parameters (Ra) under the fact that attractors are reached after an infinite time and everything is complicated by bifurcations?**
- **How to deal with spectra of intermittent signals?**
- **How to quantify chaoticity of chaotic solutions (attractor dimensions)?**

Wavelet spectra: A tool for analysis of local chaoticity

The Lyapunov exponents, the correlation matrix as well as the Fourier spectra of a selected quantity yield the characteristics of the studied system global behavior ($t \to \infty$). Intermittency can be present during its evolution or chaotic behavior can be limited to only a finite time interval, which can hardly be revealed by the global methods. Moreover, synthetic models are usually finite, which brings problems with evaluation of $\lim_{t\to\infty}$. This is the reason why a method, which is able to reveal a multiscale contents in analyzed signal on a neighbourhood of a fixed time t^0 can be highly desirable.

In the last decades the multiscale analysis by means of *wavelets* became very popular in various physical and technical applications. There are many textbooks and papers on wavelets, e.g. (Kaiser,1994; Daubechies, 1992). A review of geophysical applications of wavelets can be found, e.g., in Kumar and Foufoula-Georgiou (1997).

Here we will demonstrate how wavelets yield the multiresolution analysis of the space $L_2(E_1)$ to make it clear that the decomposition of a time series into a wavelet basis yield the information about the power of the signal on different scales in different times.

Let $\psi(t)$ be a real function from the Hilbert space $L_2(E_1)$ with the scalar product $<f|g>_{L^2}= \int_{E_1} f(t)g(t)\,dt$ and let m and n be numbers from the set of integers Z. The *translation operator* T^n is defined by the relation

$$T^n(\psi) = \psi(t-n) \tag{43}$$

and the *dilatation operator* D^m is

$$D^m(\psi) = 2^{-\frac{m}{2}}\psi(2^{-m}t)\ . \tag{44}$$

Both operators are the isometries, i.e., $||T^n\psi||_{L^2} = ||D^m\psi||_{L^2} = ||\psi||_{L^2}$, but they do not commute as $D^mT^n = T^{2^m n}D^m$.

A function $\phi(t)$ is called *scaling function*, if the functions

$$\phi_{m,n}(t) \equiv D^mT^n\phi(t) \tag{45}$$

are orthonormal for each fixed m, if

$$\int_{E_1} \phi(t)\,dt = 1\ . \tag{46}$$

and if the sequence of spaces $\{V_m \subset L_2(E_1)\}_{m=-\infty}^{\infty}$

$$V_m = \text{span}\,\{\phi_{m,k}(t), k \in Z\} \tag{47}$$

satisfies

1. $V_{m+1} \subset V_m$,
2. $P_m(f) = 0 \;\; \forall f \in L^2(E_1)$, $\;\; m \to \infty$,
3. $P_m(f) = f \;\; \forall f \in L^2(E_1)$, $\;\; m \to -\infty$,

where P_m is the projection operator onto the space V_m. The sequence of spaces $\{V_m\}_{m=-\infty}^{\infty}$ is called the *multiresolution analysis* of $L_2(E_1)$.

Define the spaces W_m by the relation

$$V_{m-1} = V_m \oplus W_m \tag{48}$$

and denote by Q_m the orthogonal projection onto W_m. Moreover, define the operators

$$H = D^{-1}P_1 \;, \quad G = D^{-1}Q_1 \;, \tag{49}$$

and their adjoints

$$H^* = DP^0 \;, \quad G^* = DQ^0 \;. \tag{50}$$

If we consider them like the operators between the spaces

$$H : V^0 \to V^0 \;, \quad H^* : V^0 \to V^0 \;, \tag{51}$$

$$G : V^0 \to W^0 \;, \quad G^* : W^0 \to V^0 \;, \tag{52}$$

we may write

$$H^*(\phi) = \sum_n h_n T^n(\phi) \ , \tag{53}$$

$$G^*(\psi) = \sum_n g_n T^n(\phi) \ , \tag{54}$$

where $\{h_n\}$ ($\{g_n\}$) are called *low-pass (high-pass) filter coefficients* and

$$\psi = D^{-1} \sum_n g_n T^n(\phi) \tag{55}$$

is the *mother wavelet*. The functions

$$\psi_{m,n}(t) \equiv D^m T^n(\psi) \tag{56}$$

are called *wavelets* and it holds that

$$W_m = \text{span}\left\{\psi_{m,n}, n \in Z\right\} \ . \tag{57}$$

Since

$$L_2(E_1) = \bigoplus_{m=-\infty}^{\infty} W_m \ , \tag{58}$$

the decomposition of time series into wavelets represents the natural way of time-scale analysis.

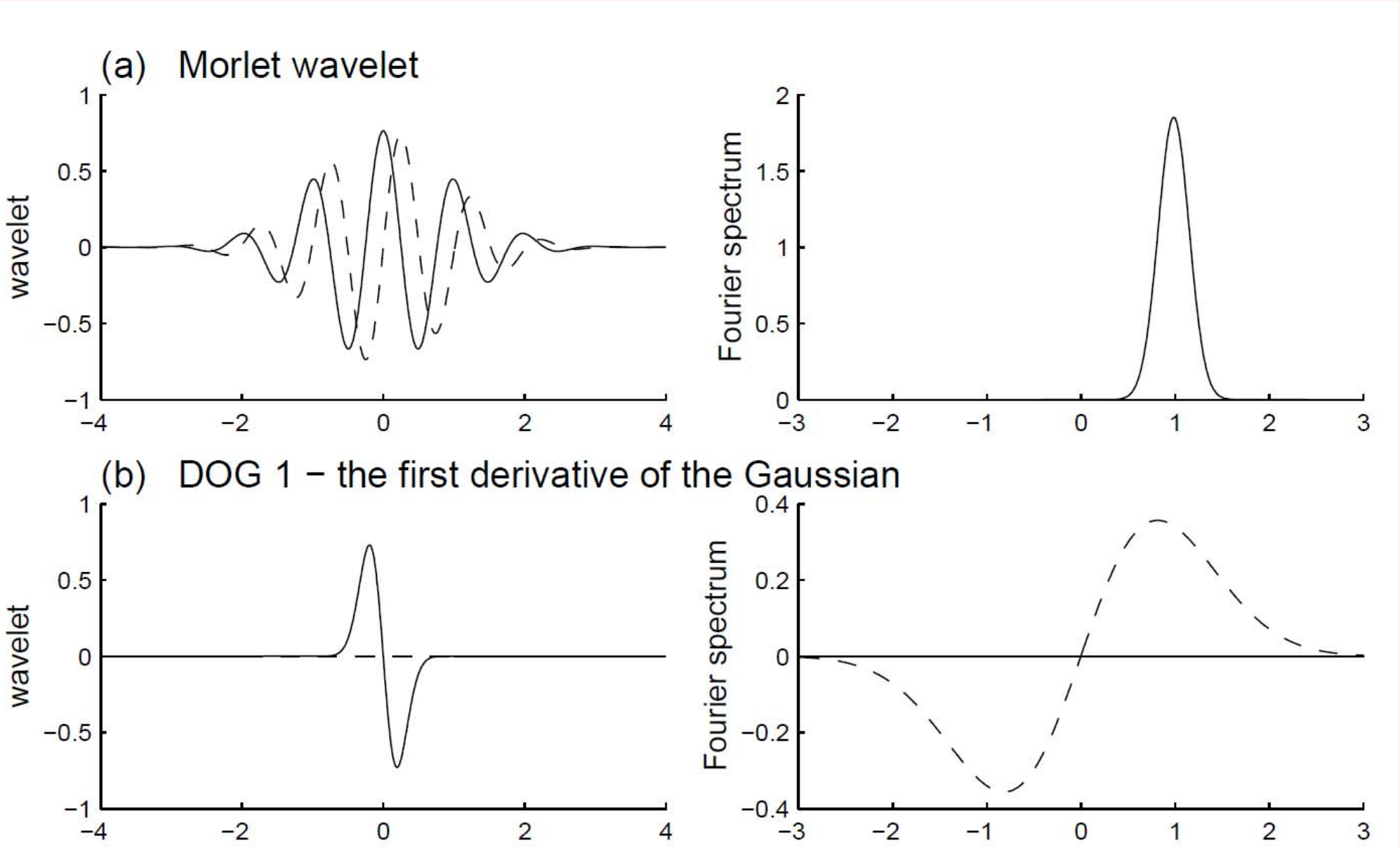

Figure 15: Solid lines—real parts, dashed lines—imaginary parts. From *Vecsey, PhD Thesis, Fac. Math. and Phys., Charles Univ., 2002.*

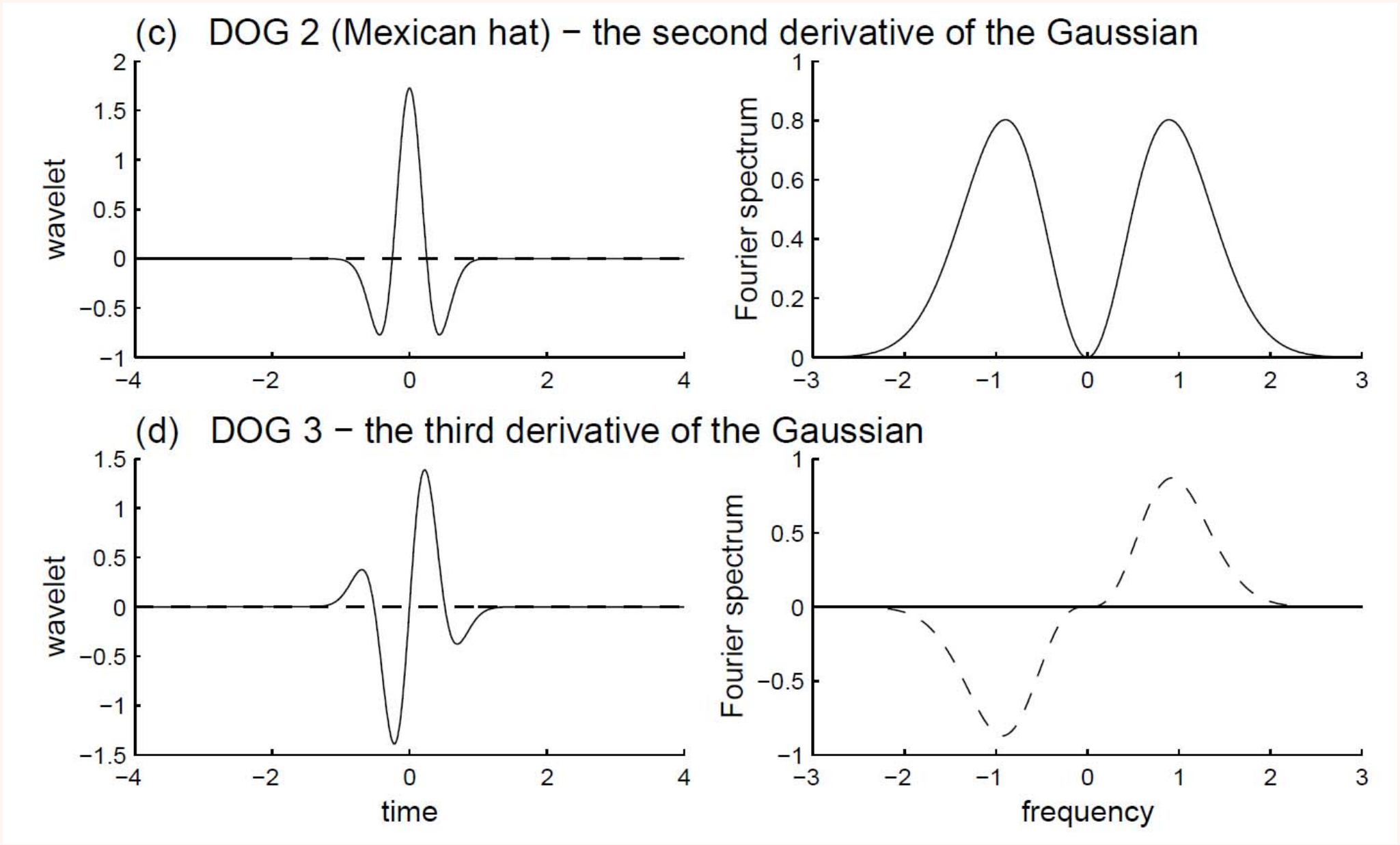

Figure 16: Solid lines—real parts, dashed lines—imaginary parts. From *Vecsey, PhD Thesis, Fac. Math. and Phys., Charles Univ., 2002.*

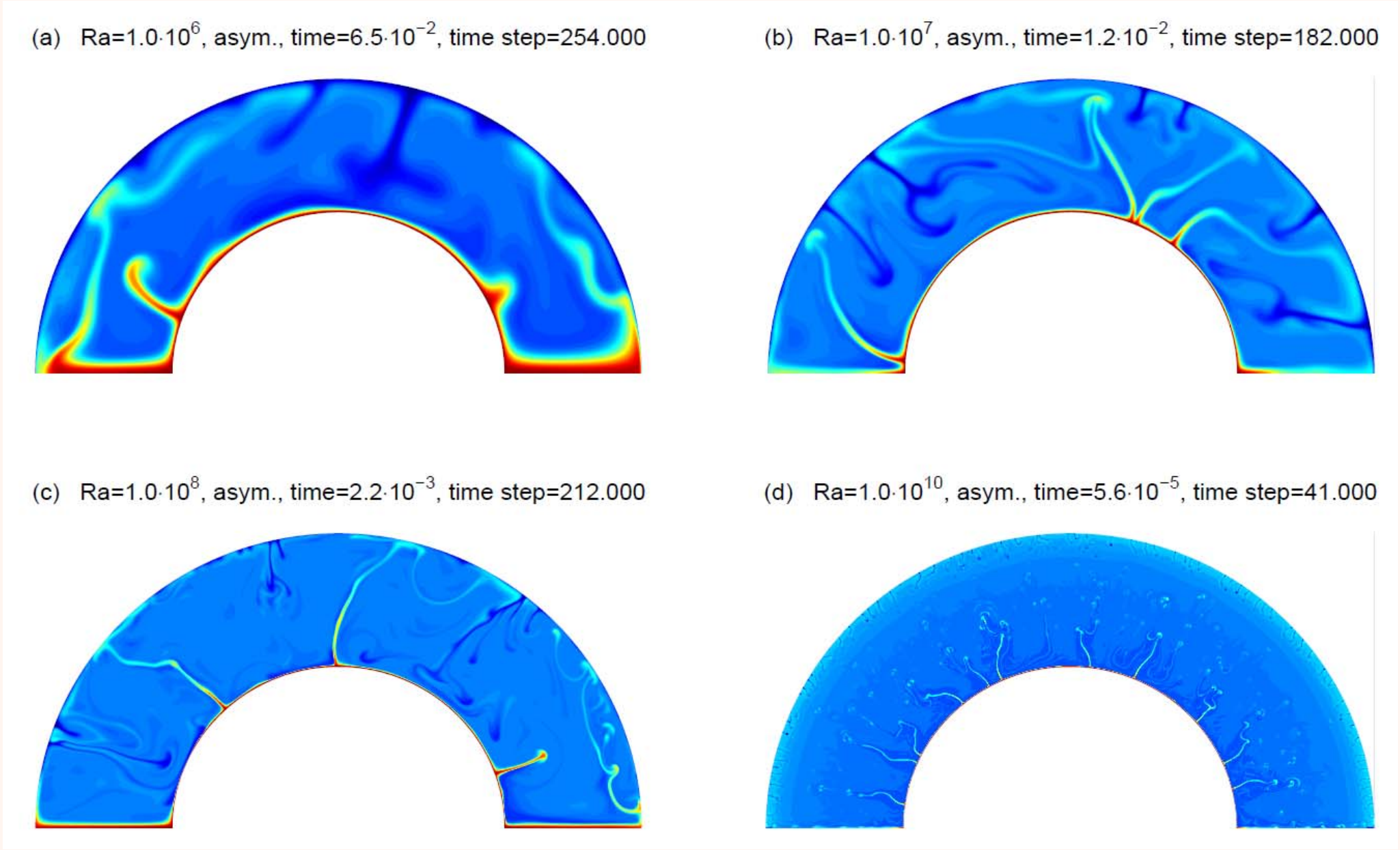

Figure 17: From *Vecsey, PhD Thesis, Fac. Math. and Phys., Charles Univ., 2002.*

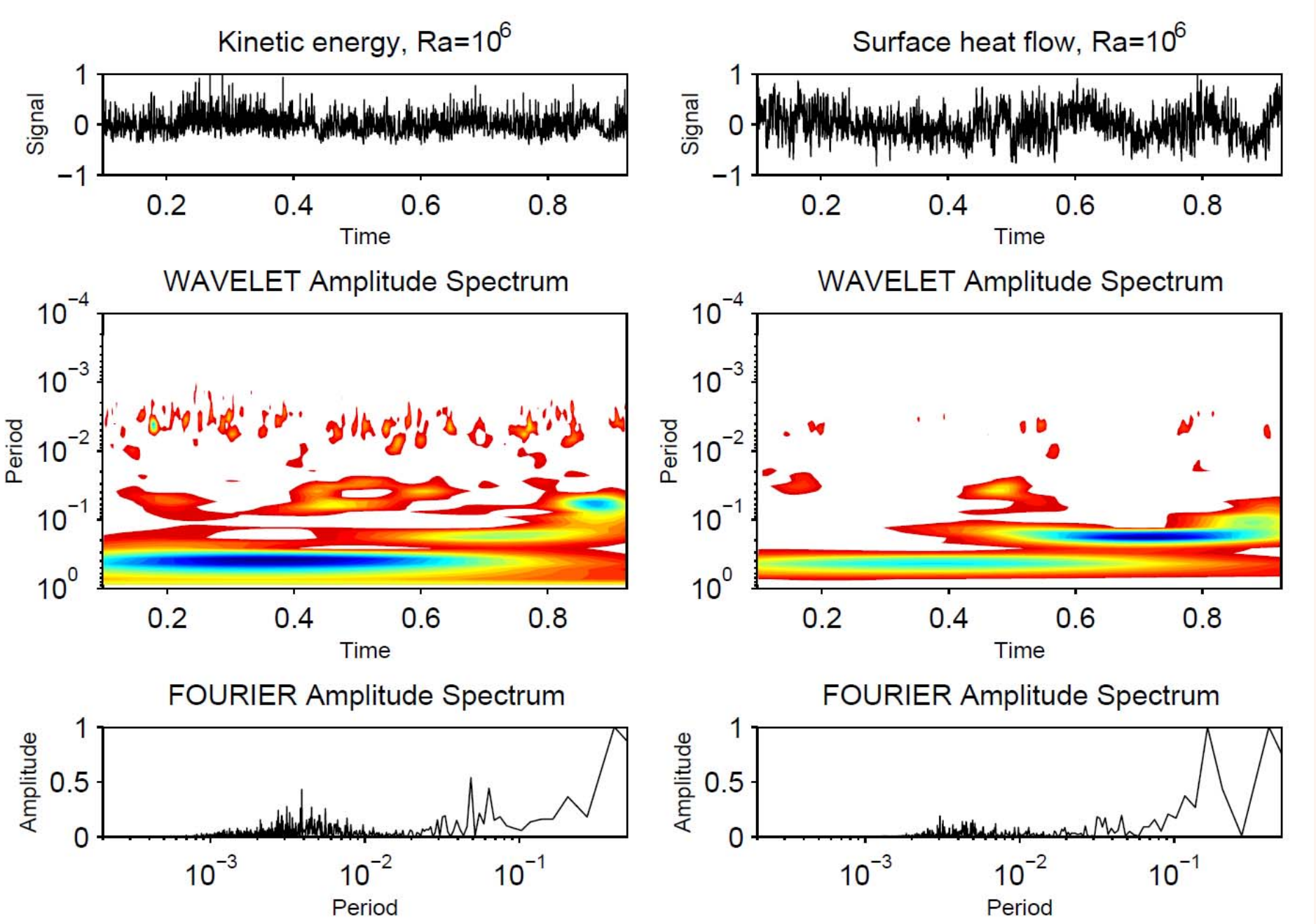

Figure 18: From *Vecsey, PhD Thesis, Fac. Math. and Phys., Charles Univ., 2002.*

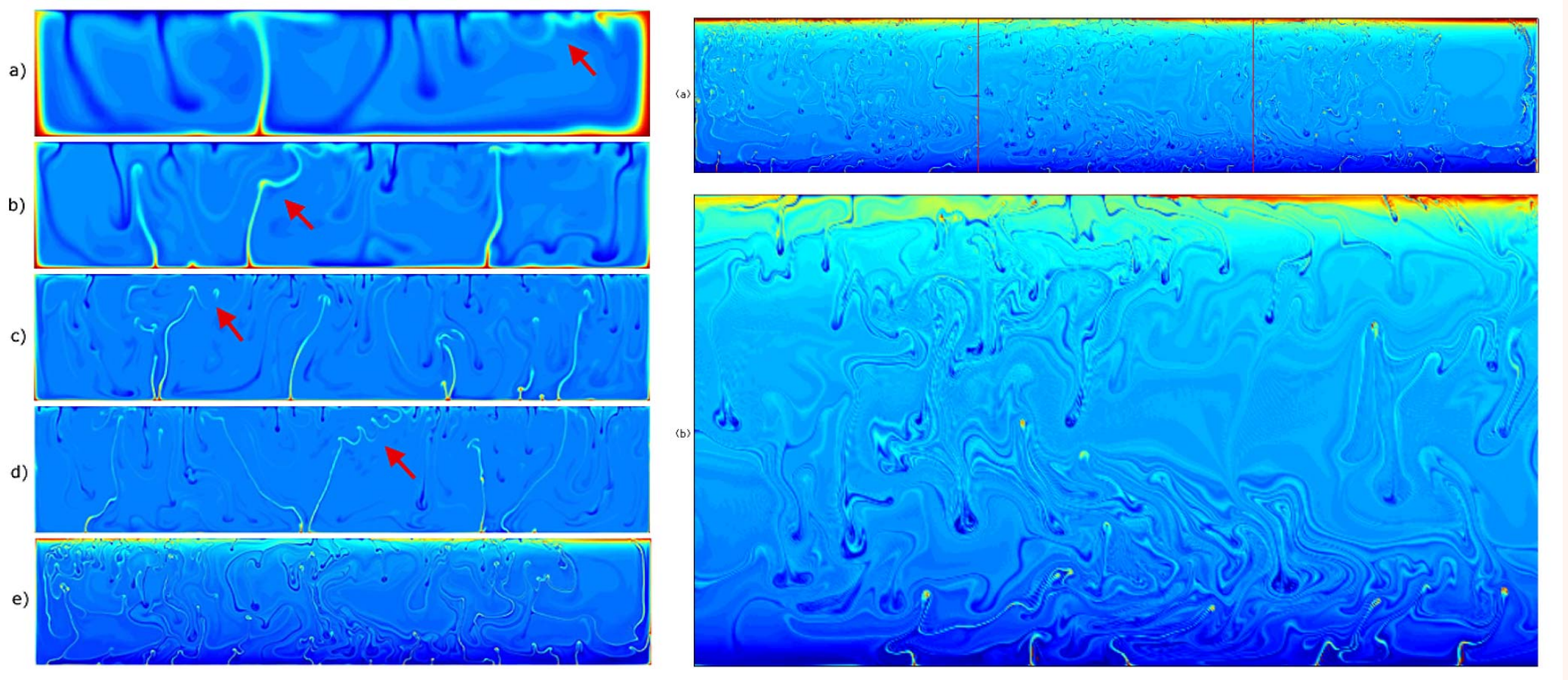

Figure 19: Rayleigh numbers: Left (a) 3×10^6, (b) 3×10^7, (c) 3×10^8, (d) 10^9, (e) 10^{10}; Right 10^{11}. From *Vecsey, PhD Thesis, Fac. Math. and Phys., Charles Univ., 2002.*

IV. Remaining questions for those studying Earth-similar complex systems

- How to deal with zoology of (stable) stationary solutions?
- How to perform transition from periodic to chaotic solutions for continuos changes of parameters (Ra) under the fact that attractors are reached after an infinite time and everything is complicated by bifurcations?
- How to quantify chaoticity of chaotic solutions (attractor dimensions)?

References

Arnold, V.I., *Mathematical Methods of Classical Mechanics*, Springer-Verlag, New York etc., 1989.

Daubechies, I., *Ten Lectures on Wavelets*, SIAM, Philadelphia, 1992.

Guckenheimer, J. and P. Holmes, *Nonlinear Oscillations, Dynamical Systems and Bifurcations of Vector Fields*, Springer-Verlag, New York etc. 1983.

Kaiser, G., *A Friendly Guide to Wavelets*, Birkhauser, Boston, 1994.

Keers, H., F.A. Dahlen and G. Nolet, Chaotic ray behaviour in regional seismology, *Geophys. J. Int.*, 131, 361–380, 1997.

Kumar, P. and E. Foufoula-Georgiou, Wavelet analysis for geophysical applications, *Reviews of Geophys.*, 35, 385–412, 1997.

Lanford, O.A., Strange attractors and turbulence, in *Hydrodynamic Instabilities and the Transition to Turbulence*, H.L. Swinney and J.P. Gollub eds., Springer-Verlag, Berlin etc. 1981, pp. 7–26.

Lappa, M., *Thermal Convection: Patterns, Evolution and Stability*, John Wiley & Sons, Chichester, 2010.

Marek, S. and I. Schreiber, *Chaotic Behaviour of Deterministic Dissipative Systems*, Academia, Praha 1991.